UNIVERSITA' DEGLI STUDI DI PADOVA
Facoltà di Scienze
Facoltà di Ingegneria

ISTITUTO NAZIONALE DI FISICA NUCLEARE
Laboratori Nazionali di Legnaro

Con la Federazione Regionale degli Industriali Veneti

Tesi di MASTER in
"Trattamenti di Superficie per l'Industria"

Application of Magnetron Sputtering Techniques to Development Contrast Details Test Objects for Mammography

Relatori: Ing. Paolo Favaron
Dott. G. Gennaro
Prof. V. Palmieri

Candidato: **Dott. Judilka Bermudez**

Anno Accademico 2004/05

Introduction

How mammography is related to Sputtering

In the past few decades a large amount of attention has been given to health service's technology. Advances in electronic components, computer technology, and images processing have contributed considerably to the expansion and improvement of the field. However, there is evidence that several other related topics still need to be explored, such as X-ray imaging in the routine mass screening for medical diagnosis.

Tumors formation is one of the most common human health problems and large efforts have been undertaken world wide to tackle the disease. Breast cancer specifically seems to affect a large percentage of the female population. Research indicates that breast cancer treatment is most effective if the disease is diagnosed in its early stages of development. Traditionally, X-ray technologies have been used for breast screening film mammography and its success in detecting breast cancer has been reconfirmed throughout the past few decades.[1] However, the technique has several limitations, and further improvements are required if we wish to achieve early stage diagnosis.[2]

Image formation in radiological diagnosis is the result of the complex interdependence of many factors.[3] Creating an ideal balance among them could improve the image to such a degree that it could be used in a clinical setting, where the minimum radiation dose would be applied to the patient.[4] The factors which increase radiation dose and affect image quality can be grouped as: radiation quality, photon intensity, X-ray detection sensitivity, and reduction of background through scattered radiation. Optimum performance is dependent on the improvement of the assessments of these phenomena.

In the past, standard methods of quality control have been introduced which have lead to a partial improvement in the image evaluation techniques. Some methods, widely applied, involve the use of test objects or *phantoms* for the establishment of comparison parameters[5,6]. However, the methods that use phantoms, are frequently not as reliable as radiation based diagnoses of asymptomatic woman produce. In addition, the subjective nature of image interpretation by medical professionals can make the assessment process very difficult. Consequently, the currently available tools which are used for breast clinical image formation and interpretation regularly results in an incorrect diagnosis.

In past years, the commercially introduced *digital detectors for mammography* were seen as an important advancement since they provided both a higher acquisition speed and a lower associated radiation dose. However, up until this point, the quality of the produced images is comparable to the images obtained with film detectors. Even though applying a lower dose represents a great advantage, there is no improvement in image quality production. In addition, has been demonstrated that using traditional phantoms, to evaluate image quality on digital mammography, did not bring enough information about certainties on dose measurements.

But a new window is open for innovation, since dose control on digital mammography systems depends on factors where major improvement can be achieved.[7] Theoretically, it is possible to enhance discriminating threshold and therefore improve image interpretation at a higher degree. Although at the moment it has still not been achieved, it is within reach since there is currently underway the development of new instruments which have a better approach for the assessment of digital mammography systems.[8] We propose one of the improvements.

The construction and research of the uniformity and replicability of a *contrast detail test object* could represent an advance in this research field. Until now, a phantom use for digital mammography has not been provided, that can provide both uniformity and reproducibility such that it could be used as a main interpretational tool. This knowledge would allow for the establishment of standard parameters in both the systematic and even automated recognition of abnormal breast formations

The aim of this work is to apply magnetron sputtering technique in the development of a *contrast detail test object* for digital mammography, assuring uniformity and reproducibility within the requested constrains to the preparation and analysis of them.

Recently physical vapor deposition techniques (PVD) have been proposed, which are well known in the field for thin film preparation.[9] This technique, reported for the first time in 1852, when a metal was sputtered from the cathode of a glow discharge, has become one of the most advantageously applied in semiconductor manufacturing and generally in the electronic industry.

In thin film deposition and growth, sputtering provides reliable control of thickness, high adhesion and good morphology. The technique is flexible and can be applied for several types of substrates as polymers, metals, and ceramics among others. In addition, thickness can be controlled in situ during growth stet and therefore a greater uniformity of coating can be achieved.

Using sputtering process is possible to deposit, over a flat substrate, thin films of high X-ray absorption material, with specific shapes. Such a sample could be used as the *contrast detail test object* of the phantom for mammography. Our proposal of using magnetron sputtering for fabricating contrast detail test object construction seems to adequately satisfy the quality requirements, the reproducibility, and the uniformity. As a consequence, sputtering may arise as the best selection for their development. Due to the previously mentioned advantages of preparing a proper phantom, sputtering will be a key aspect of this study.

The development of this thesis has been carried out following an experimental methodology, which purposes a new phantom for digital mammography. Based on the literature review, presented briefly in chapters 1 and 2, we established the possible materials with the adequate characteristics for the construction of the *test object*. Simulations of X-ray attenuation were carried out on different phantoms configurations varying elemental composition as well as thickness for each constituent. At the same time, design of the geometrical characteristics of the contrast detail test object and the mask needed to achieve it, were done.

Base on the simulations results, we selected the components materials and the configuration of the phantom. Deposition of tungsten over flat quartz showed the optimums attenuation results, satisfying both: phantoms requirements with respect to the X-ray attenuation and feasibility. Sputtering parameters were studied in order to obtain tungsten thin films with thickness required. Pressure, target-substrate distance and power supply were optimized to achieve the necessary adhesion, shape and thickness parameters. Tungsten was deposited in several thicknesses. Analyses of borders, mask effect and uniformity of the deposition were done. Analysis of reproducibility of the *contrast detail test object* was also carried out and the results and discussion are presented. Further work is proposed, and preliminary results of the progress on it are presented on the last chapter.

This thesis can be seen as a starting point to make further inquiries into the field of material science and its potential ability to contribute to mammography methods and research. Once more, material science offers alternative techniques with the versatility to provide solutions for growing research fields, such as the assurance of X-ray mammography quality. This could therefore lead to an improved health care unit, especially since the new phantom is within reach. It should be considered as an innovative contribution to the field.

CHAPTER 1

Mammography: Literature review

In this chapter, aspects of mammography main topics, the characteristics of X-ray and required radiation dose will be shown. Further, the mammography detectors and the relevance of phantoms for contrast detail are given.

Mammography is a specific type of medical imaging that uses a low-dose X-ray system for breast examination. Mammography is also used as a screening tool to detect early breast cancer in asymptomatic women. This kind of exam plays a central part in the early detection of breast cancer, since it may show tissue changes in the human breast, up to two years before a patient or physician may diagnose them. In fact, mammography screening is recommended every year for women, beginning at age 40. Studies have shown that annual mammograms are most efficient in the early detection of breast tissue abnormalities, since this is the stage when they are most curable and breast-conservation therapies are most effective.

Despite mammography being the most effective technique for early breast cancer detection, it still runs the risk of producing both false-negatives and false-positives, with false-negatives being the more frequent of the two.

Therefore, further research in this field is currently in progress and a variety of breast imaging techniques are going to be explored in order to improve mammography sensitivity and specificity. This advancement would quickly increase diagnosis accuracy. The results of the studies obtained with phantoms may provide much sought after improvement. This study attempts to produce an object that may contribute to the enhancement of various aspects of the field.

1.1 Characteristics of Mammography

A mammography unit is essentially a system for X-ray radiography dedicated exclusively for breast exams. This unit includes some special accessories such as beam collimator to confine X-rays to a small region of the body so to limit the exposure to ionizing radiation. A compression paddle is included to keep approximately the same thickness of the breast during the imaging process and also to reduce the effect of scatter radiation as much as possible.

Fig. 1.1: Digital mammography system.

The two major components of the system are the X-ray tube and the image recorder. The first generates the electromagnetic beam that is partially transmitted through the breast. The second is a screen/film cassette or a digital detector that provides a projection image of breast tissue density. The mammography systems available today are specifically designed and optimized to detect breast anomaly given by dark-grey gradients on image. This certainly would improve if image interpreting was digitally processed with more innovative techniques i.e. introducing new phantoms that would allow for the establishment of systematic quality control with a low level of uncertainties.

1.2 X-ray for mammography basics

X-ray beams used in mammography are produced when electrons emitted from a cathode are accelerated against a rotating anode, typically made of molybdenum. X-ray energy distribution, including both characteristic and bremstralumg radiation, is represented by the X-ray spectrum, as shown in Fig. 1.2. The spectrum emitted is usually filtered with molybdenum or rhodium to absorb low energy x-rays (few keV) which are useless for image formation and would increase the patient dose, and increase the relative intensity of characteristic peaks.

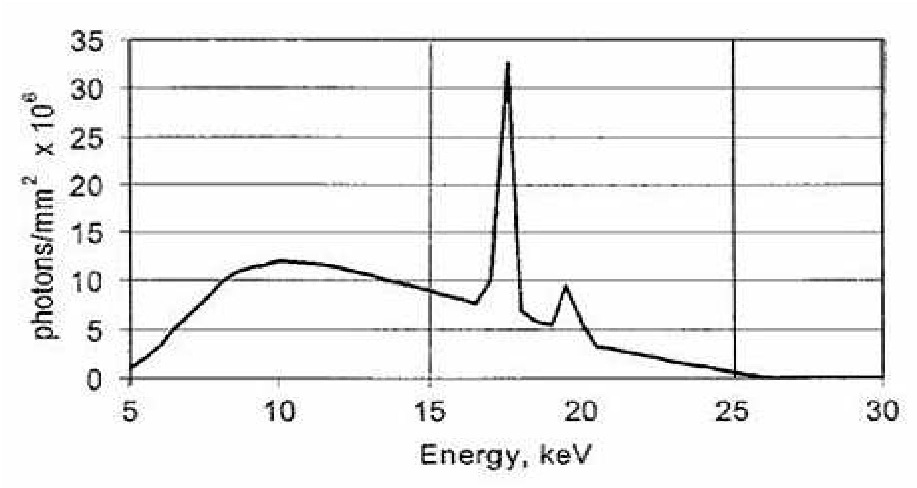

Fig. 1.2: Unfiltered Bremstralumg spectrum using a Mo target at 26 kV showing superimposed peak due to the anode material.

Molybdenum shows characteristic peak, K line, at 17.48 keV ($K\alpha_1$), 17.37 keV ($K\alpha_2$), 19.61 keV ($K\beta_1$) and 19.96 keV ($K\beta_2$). The use of molybdenum filters (Mo/Mo combination) enhances an important effect for image resolution by preferentially attenuating photons in the energy region around 10 keV and above 20 keV.

The other effect that determines spectrum shape is the voltage value applied between anode and cathode that determines the end point of the spectrum, an example given in Fig. 1.3 is a representative case. Voltage affects also the mean energy of the spectrum and the tube output intensity. In fact small voltage changes may improve the quality of mammography image depending on material attenuation property. Therefore, changing the applied voltage is one of the techniques that skilled operator apply to improve effectively image contrast.

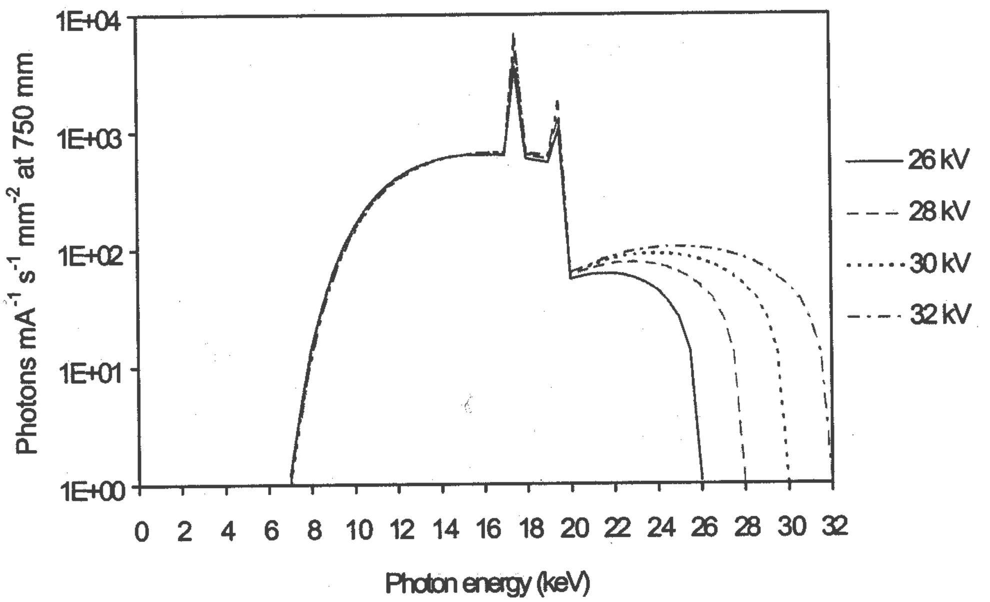

Fig. 1.3: Effect of varying applied voltage on simulated molybdenum spectra.

Further advantage could be gained by adjusting the signal-to-noise ratio parameter since breast imaging depends also on the compressed breast thickness. Experimenting with different materials, particularly for thick breast, where use of Mo anode with Mo filter risk underexposition, and consequently acquisition of a poor contrast image, has been determined that contrast improves by replacing the molybdenum filter with rhodium or palladium within the alternatives of rhodium target as anode.

Spectra produced with rhodium targets (Rh/Rh combination) exhibit K line at the energies of 20.07 keV (Kα1), 20.21 keV (Kα2). The characteristics of these target elements can be discerned from the curves given in Fig. 1.4. Moreover, use of Rhodium anode and filter implies increasing of energy that aims to diminution of dose applied to the patient. However, the agreement between contrast image and radiation exposure have to be accomplish, due to increasing on energy entails loose of contrast image quality.

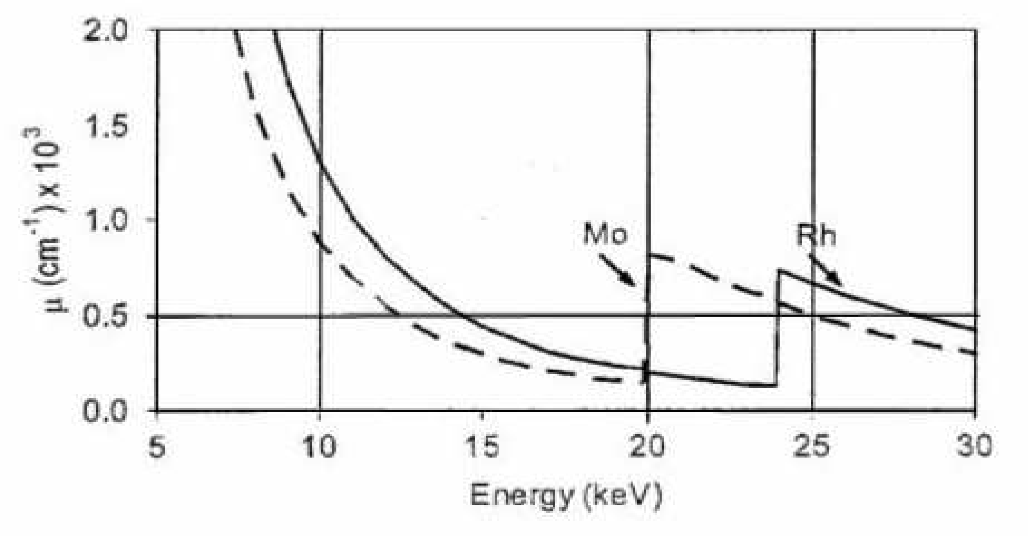

Fig. 1.4: Linear attenuation coefficient (μ) as function of energy for Mo and Rh target.

1.3 Breast X-ray imaging

The breast is mainly made of adipose, fibrous and glandular tissue and these tissues have different radiosensitivity that must be taken into account during imaging protocol. As mentioned before, the breast is exposed to a dose of radiation adequate to obtain an image with enough contrast so that the internal breast tissue can be discriminated. In Fig. 1.5 we present a diagram of the main section of the mammary gland. A breast mammogram is a "grayscale map" of the x-ray beam transmitted through the breast, which could be recorded by a film (previously amplified by a luminescent screen) in conventional mammography, or by a digital detector in digital mammography. Often large sets of images are produced with the purpose of defining a window of values to assure a relatively good image at the achievable lower dose.

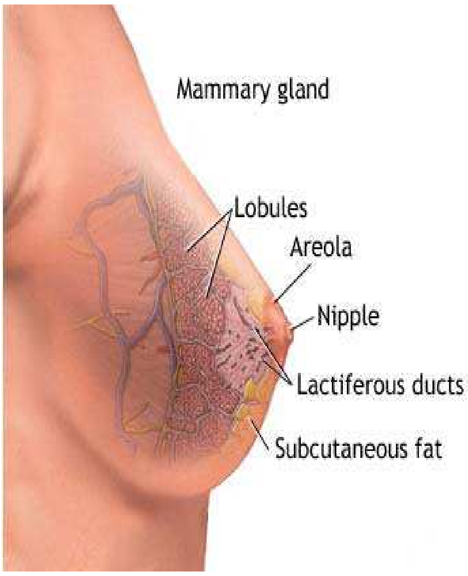

Fig. 1.5: Breast scheme illustrating the main parts.

The process of generating an image specific enough to recognize small lesions embedded in soft tissue is one of the principle objectives of mammography. Often, due to technical difficulties, effects of physical parameters as well as exposure and other several factors (upon which image analysis improvement may be sought), resulting images are not completely satisfactory. Each breast tissue type has a specific radiation attenuation determined by physiological factors.

In order to illustrate the attenuation of breast components, as adipose tissue and glandular tissue, chemical composition for this tissue types are given in the Table 1.1.

Table 1.1: Elemental composition of beast tissues[10].

Composition	Adipose tissue mean %	Adipose tissue range %	Glandular mean %	Glandular tissue range %
Hydrogen	11.4	11.2 - 11.6	10.6	10.2 – 10.9
Carbon	59.8	51.7 - 68.1	33.2	15.8 – 50.6
Nitrogen	0.7	1.3 - 0.2	3.0	2.3 – 3.7
Oxygen	27.8	35.5 – 19.8	52.7	69.8 -35.8
Ash mineral	0.3	0.3	0.5	0.3 – 0.5
Density(g/cm^3)	0.95	0.93 - 0.97	1.02	0.99 – 1.06

Effect of chemical composition in attenuation of X-ray can be estimated using mass attenuation coefficients. This express capacity of materials to attenuate radiation and the governing physical law is an *exponential law:*

$$\frac{I}{I_0} = e^{-(\mu/\rho)x} \qquad \text{(eq 1.1)}$$

where I_o is the incident intensity, of a photons beam, penetrating a layer of material with mass thickness x and density ρ, emerges with a reduced intensity of I.

Equation (1) can be rewritten as

$$\left(\frac{\mu}{\rho}\right) = \ln\left(\frac{I - I_0}{x}\right) \qquad \text{(eq 1.2)}$$

where the ratio (μ / ρ) is experimentally determined having set I_o, I and x values.

To show some experimental values, mass attenuation coefficient μ/ρ *(cm²/g)* for major human body compounds, is given in Fig. 1.6.

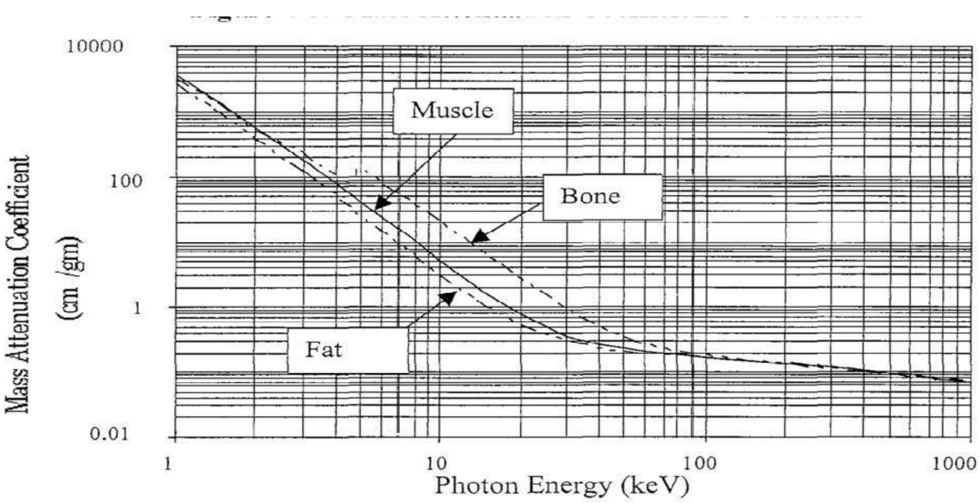

Fig. 1.6: Mass attenuation coefficient for major human body compounds.

Generally speaking, radiography analyses, only to a certain degree, supplies medically useful information about both healthy and unhealthy tissues which have different densities. The Fig. 1.6, shows how the attenuation of bones and fat produce images which are easily distinguishable since they are presented in the radiographic images with a high gradient of dark-grey shadow. However, the breast proves to be just the opposite because it is an organ with an intrinsic low contrast. The adipose and the glandular tissue, due to the similar attenuation coefficients, make difficult or at least less immediate to make the distinctions between them. Therefore having similar densities introduce a limitation in both image definition and also in the capacity to identify small differences between the tissues. The Table 1.2 provides a list of physical properties which supports this observation on of breast tissue discrimination.

Table 1.2: Physical properties of Human Body constituents.

Tissue type	Linear attenuation Coefficients (μ) Mean (cm^{-1})	Linear attenuation Coefficients (μ) Range (cm^{-1})	Mass energy absorption Coefficient (μ_{en}/ρ) Mean (cm^2g^{-1})	Mass energy absorption Coefficient (μ_{en}/ρ) Range(cm^2g^{-1})
Adipose	0.546	0.502 – 0.590	0.332	0.299 – 0.363
Gland	0.713	0.613 – 0.819	0.449	0.374 – 0.518

In Table 1.2 demonstrates again how the low attenuation makes it more difficult to improve image contrast for breast analysis than compared to the tissues reported in Fig. 1.6.

The mass attenuation coefficient μ/ρ determine the characteristic absorption of material. The energy **E** of the X-ray beam determines the value of the mass attenuation coefficient (see Fig. 1.7) and is one of the most important factors in controlling both the radiographic and overall (image) contrast.

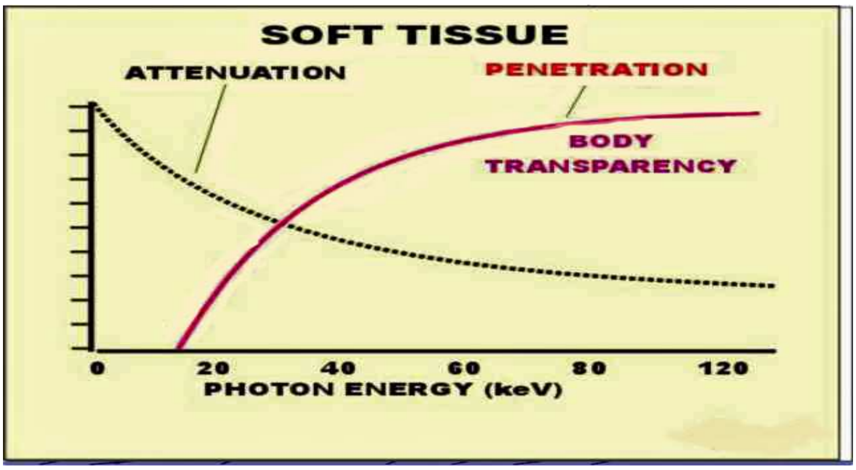

Fig. 1.7: Variation of attenuation and penetration in function of energy.

Breast masses (including benign and cancerous lesions) appear as white regions on a black background. Fat appears darker on a dark-grey gradient regions on a mammogram image. Everything else (glands, connective tissue, tumours and other significant abnormalities such as micro-calcifications) appears as levels of white as shown in Fig. 1.8. Here, white spot shape and size is the most determining factor to establish early stage of unwanted growth.

Fig. 1.8: A typical abnormal breast image showing details of different tissue density.

1.4 Breast radiation exposure

Estimating the amount of dose absorbed by the breast is an important aspect of monitoring the mammography's quality. Breast dose is also a key parameter in the evaluation of developments in mammographic imaging systems, the comparison of performance at different centers and the establishment of local, regional and national standards.[11]

The dose, to the whole breast, depends strongly on the X-ray spectrum, the breast composition and the breast thickness. Any scheme for estimating breast dose should therefore provide a measure of the average dose to the breast tissue rather than entrance dose. Any scheme for estimating the dose based on test phantoms should use materials of appropriate composition.

Karlsson[12] et al. suggested that the mean dose to the glandular tissues within the breast would be the best measure of risk. Significant fractions of the energy absorbed by the breast are deposited in skin, fat and connective tissue; whereas it is believed that it is the glandular tissue which has the highest risk of radiation-induced carcinogenesis. Mean glandular dose (MGD) is the quantity recommended by the ICRP[13] and is used in many national protocols i.e. European Protocol, 1996.

The mean glandular dose (MGD) is given by[14]:

$$D = K_f\, g \qquad \text{(Eq. 1.3)}$$

Where g: is the conversion factor usually expressed in units of mGy/mGy,

K_f : is the incident air kerma at the breast surface measured free in air.

The mean glandular conversion factor can be estimated using Monte Carlo modeling of the mammographic examination, taking in account the differences of mass absorption coefficients of breast tissues and their respective risk associated. The kerma spectrum is the photon energy distribution (photon spectrum) or dose energy distribution. Kerma in air is defined as the kinetic energy transferred to ionizing particles per unit mass of air by indirectly ionizing radiation. The air kerma at the point of entry of the breast, K can be estimated from knowledge of X-ray tube output, the compressed breast thickness, the distance from the focus to the breast support plate, and the exposure parameters used.

1.5 Detectors for digital mammography

In a mammography, the X-ray source radiates through the compressed breast and onto a film cassette or digital detector positioned under the breast.

In *film mammography*, which has been used for over 35 years, the image is created directly on a film. While standard film mammography can be very good, it is less sensitive for women who have dense breasts and different studies have suggested that approximately 10 to 20 percent of breast cancers that were detected by breast self-examination or physical examination are not visible on film mammography. *Digital mammography* is the new technology. In this, an electronic image of the breast is taken and stored directly in a computer. Digital mammography gives fewer doses than film mammography and allows improvement in image storage and transmission since images can be stored and sent electronically. Appropriate software can help in the interpretation of the digital mammograms.

1.5.1 Film detectors

In Film mammography the x-rays hit a special screen coated with phosphorescent compound. The phosphorescent screen inside the cassette often is constructed of rare earth compounds such as gadolinium oxisulfide (Gd_2O_2S) that emit light upon absorption of X-rays. When an X-ray is absorbed, the resultant light scintillation creates a number of photons proportional to X-ray beams intensity that spread and illuminates the film in a distribution cloud. Film near the screen captures the photons and the image of the internal structure of the breast is obtained. The resulting "exposed film" inside the cassette is then developed in a dark room.

The thickness of intensifying screen is an important parameter. For example a thicker screen absorbs more x-rays and therefore more doses efficient. But a thicker screen also creates more scattering and blurring of the image. Therefore, it is impossible to offer a screen-film system simultaneously offering the highest possible resolution and lowest possible dose.[15]

A major limitation of film mammography is the film itself. Once a film mammogram is obtained, it cannot be significantly altered; if the film is underexposed, for example, contrast is lost and cannot be recovered. In addition, film does not have a linear sensitivity to the photon flux, and there is a narrow range over which it can detect small differences on contrast. In particular, tissue areas of high and low density are often sub-optimally registered.

Films also require processing time and storage space.

1.5.2 Digital Detectors

Digital mammography, also called full-field digital mammography (FFDM), is a mammography system in which the film is replaced by solid-state detectors that convert X-rays into electrical signals. The electrical signals are used to produce images of the breast on a computer screen or printed on special film similar to conventional mammograms. There are two methods of image capture used in digital mammography: indirect conversion and direct conversion.

Indirect conversion digital detectors use a two-step process for X-ray detection. The first step requires a scintillator layer as cesium iodide doped with thallium [CsI(Tl)] to capture X-ray energy and convert it in to light. An array of thin-film diode converts photons in to electronic signals that are captured by thin-film transistors. As for to screen-film, light scatter compromises image quality, and there is a performance tradeoff between spatial resolution and radiation sensitivity.

Direct conversion digital detectors eliminate light scatter problems. In this system a photoconductor absorbs X-ray and directly generates signals. Under an external electrical field, holes, drift towards a pixel electrode and are collected on a pixel capacitor. Since the electrons and holes travel along the direction of the electric field lines, they move with lateral charge spreading. The photoconductor used in direct conversion systems is amorphous selenium (a-Se). In this, the response function maintains its sharpness even as the thickness photoconductor is increased, so there is no tradeoff between radiation stopping power and spatial resolution. In practice, the photoconductor is made sufficiently thick in order to stop the majority of the incident X-rays and this can be done without adversely affecting the spatial resolution.

There are several commercially available digital mammography detectors. The following is a list of some of full-field-of-view digital mammography detectors commercially available in the U.S (see Table 1.3).[16]

Table 1.3: Indirect-conversion detectors.

• GE
Scintillator CsI(Tl) Pixel size TFT 100 microns Field of view 18 x 23 cm
• Fischer Imaging
Scintillator CsI(Tl) Pixel size CCD 24/48 microns Field of view 22 x 30 cm (scanning) Direct-conversion detectors
• Hologic/Lorad
Photoconductor amorphous selenium Pixel size TFT 70 microns Field of view 24 x 29 cm

One of the obstacles to greater use of digital mammography is its cost, with digital systems currently costing approximately 1.5 to 4 times more than film systems.

1.6 Contrast

Conceptually, image contrast refers to the difference in brightness or darkness between an area of interest and its surrounding background. For example, if grey and white dots are painted on a black canvas, the white dots present more contrast than the grey dot respect to the background (Fig. 1.9).

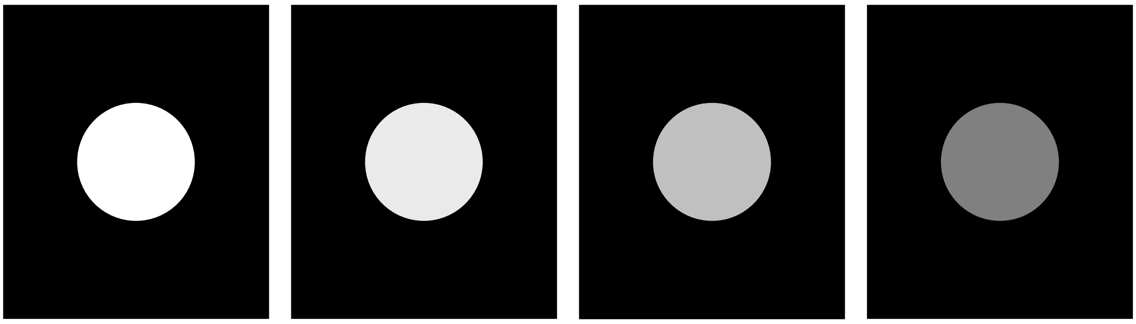

Fig. 1.9: Different levels of contrast.

The information in a medical image usually is presented in "shades of grey". Radiologists use the differences in grades shades to distinguish different tissue types, to analyze anatomical density relationships, and to compare what they see with known patterns, in order to assess the potential presence/absence of abnormality. The objective in a medical imaging is to maximize the contrast in the image for any particular region of interest; a1though this is not always possible to achieve due to design constraints where noise and spatial resolution are also very becomes more important. Grey gradients in any image depend on both material characteristics of the object being depicted and the devices used in the process.

Contrast is defined as the difference between two optical densities for film images and for digital images, is defined as the relative difference between intensities measured in the detail and in the background, relative to the background.

In medical radiographic images, different instrumental parameters influence the image contrast. In Fig. 1.10 is shown main of them, in Fig. 1.11 is presented a block diagram is given to show the influence on the image contrast of the different part involved:

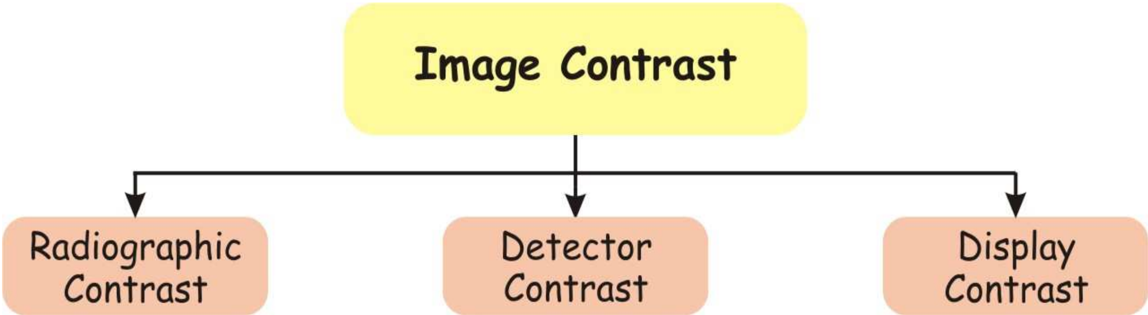

Fig. 1.10: Main Components of image Contrast

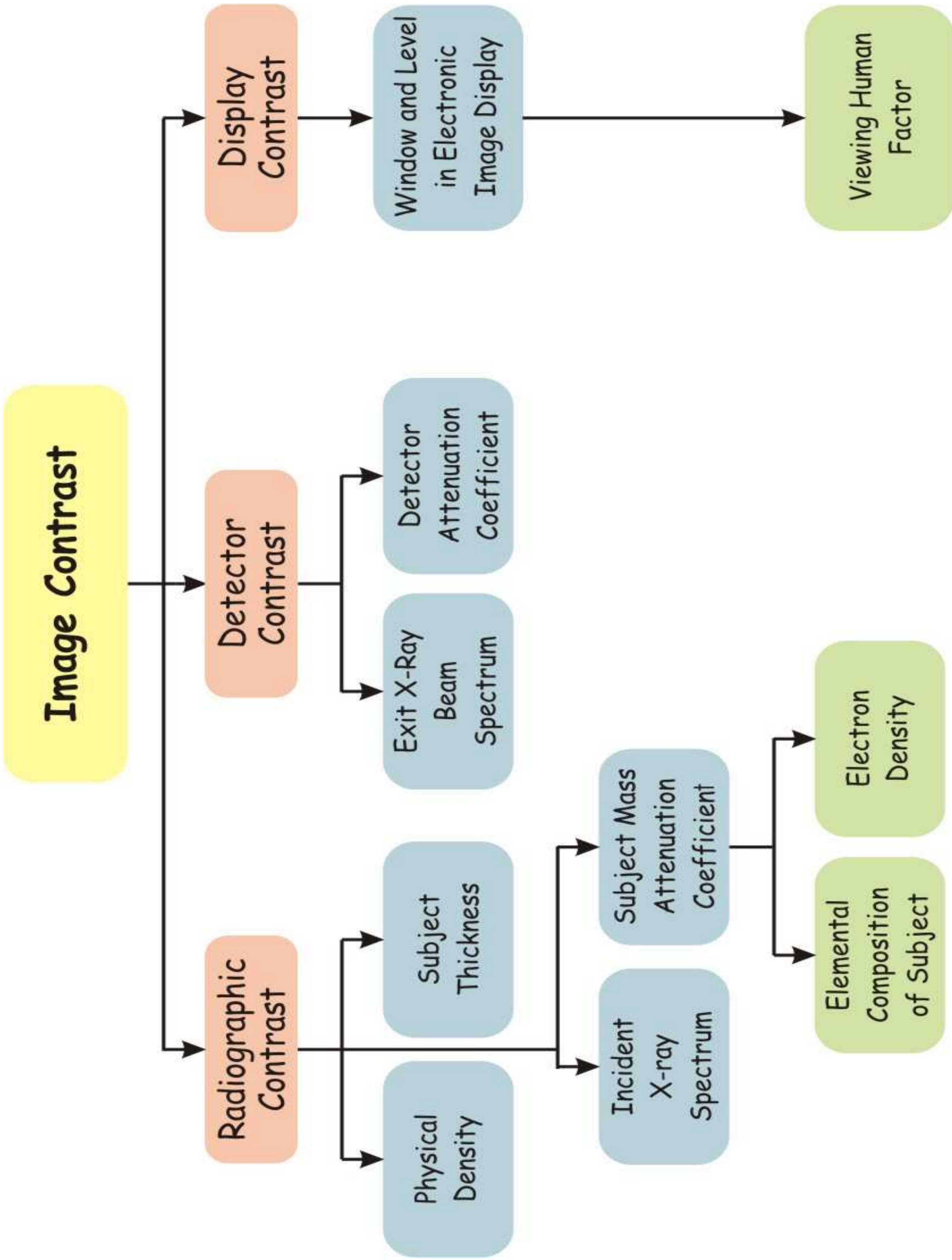

Fig. 1.11: Components of Image Contrast

In this work the improvement of *radiographic contrast* was the motivation to make the evaluations and image contrast definition. Before detail description, will be mentioned briefly the other factors that affect the image contrast.

- The *detector contrast* depends on the chemical composition of the detector, materials its thickness Δx, atomic number Z, electron density ρe, and the physical process by which the detector converts the radiation signal into an optical, photographic or electronic signal.
- Various *physical perturbations* i.e. scattered radiation and the base and fog density levels of the film affect the contrast image resulting in a reduction of its intensity.
- Operator skills, environmental factors such as the existence of high levels of ambient light in the viewing area, affect the perception of the image. Training and/or memory of similar images also impacts visual perception of the information in a radiograph.

These will not be included in further discussions. Instrumental parameters were controlled using same configurations on each exposure.

1.6.1 Radiographic Contrast

The physical determinants of contrast can be understood by examining the processes by which a radiographic image is formed. One can consider a system in which a patient is placed between an x-ray tube and a detector, the detector being either a film-screen combination or an electronic detector. X-ray tube is operating at specific kV, which, along with any filtration, determines the energy spectrum of beam. X-ray photons from the source are absorbed by the tissues in the patient (muscle, fat, air) along the path between the source and detector. Photon attenuation of each tisues depends on its elemental composition as well as the beam energy. This effect is quantified by its mass attenuation coefficient, which gives the fraction of photons that are absorbed by a mass unit of the material as demonstrated in eq 1.5.

If we could count photons on the detector-side of the patient, we could determine the radiographic contrast at this point in the image formation process. As defined before, the radiographic contrast is defined to be the fractional difference in photon flux between two adjacent areas. For example, if behind the patient, photon flux of Φ_1 is measured in one area while a photon flux of Φ_2 is measured in an adjacent area (Fig. 1.12), then the radiographic contrast is defined to be

C = Contrast

ϕ = Number of photons

$$C(\varphi) = \frac{|\varphi_2 - \varphi_1|}{\varphi_1} = \frac{\Delta\varphi}{\varphi} \qquad \text{(eq.1.5)}$$

For an opaque object, one where φ_2 is equal to zero, the contrast is equal to 1. For a uniform area where $\varphi_1 = \varphi_2$ then the contrast is equal to zero, and the object can not be differentiated from its background because they create no difference in photon flux.

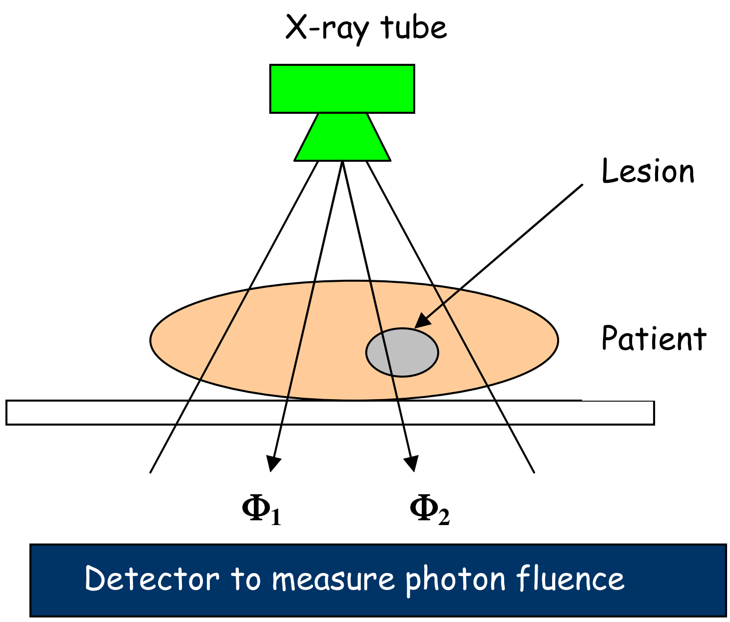

Fig. 1.12: Scheme of contrast image detection system.

The ideal set of parameters describing image quality should give a measure of the effectiveness with which an image can be used for its intended purpose, namely answering the clinical questions posed. They should therefore relate to the ability of the image to demonstrate disease and to delineate anatomical structures which are relevant to detection, deferential diagnosis and localization.[1]

1.7 Phantoms

Phantoms are test objects manufactured to define reference parameter for X-ray image acquisition and are constructed using materials that simulate X-ray attenuation of a particular organ or body part. The parameters defined in a phantom, as absorption and size; allow for the establishment of correlations with phantom images and consequently allows for the observation of both the parameters and limitations of the *real subjects* images. Phantom analysis can bring information about dose and quality of acquired image using X-ray systems.

In medical X-ray radiography, measurements of image quality are performed routinely with test objects. The techniques attempt to measure the threshold strength at which, a signal can be seen in an image. Rose[17]-Burger[18] phantom and the FAXIL test objects,[19] are objects in which simple signals, such as squares or circles, are present in regular arrays of different sizes with contrast varying regularly in one direction (Fig. 1.13(a)). An assessment of the characteristics of the X-ray system can be done by the operators. Based on the perception of the image, resolution and contrast can be evaluated using phantoms i.e. resolution can be measured from a line pair test object containing groups of metal strips with a variety of widths and spacing as shown in Fig. 1.13(d) and a measure of threshold contrast can be measured from an array of discs of varying contrast shown in Fig. 1.13(b).

The observers should be able to indicate the lowest contrast signal of each size that is visible. These tests provide information on imaging capability at different doses or dose rates through visual assessment. They do not provide information on the performance of the system for different radiation qualities or amounts of scattered radiation relating to clinical use, although the system sensitivity may vary with radiation quality.[20] Similar methods can be used to optimize particular aspects of an imaging system, such as the photon fluence (optical density on the film) required for image perception.[21]

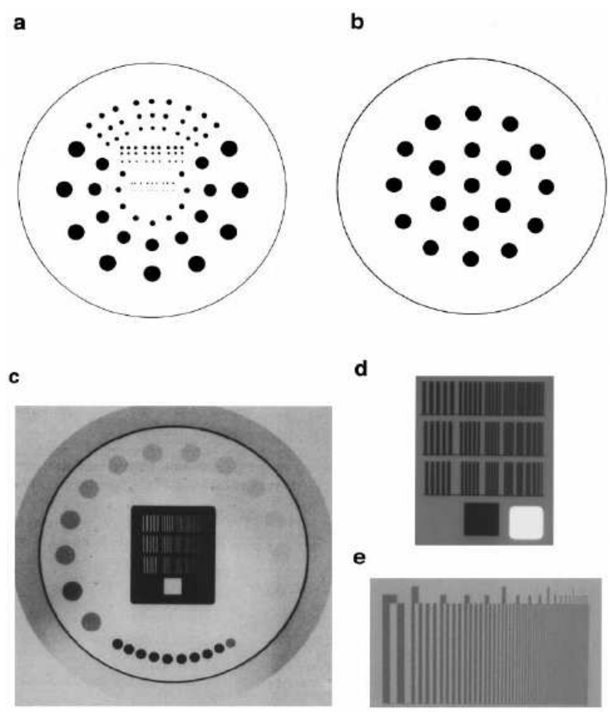

Fig. 1.13: Different test objects images.(a) contrast detail, (b) threshold contrast for fluoroscopic units, ((c) TOR object for film screen radiography. (d) Hunter line pair test object and (e) a line pair object.

In mammography, are used standard test object for X-ray radiography. There are not test objects with attenuation similar to these generated by real breasts. A standard breast was defined as 4.5 cm thick with a 0.5 cm adipose shield and a central region composed of equal parts by weight adipose and glandular tissue. In the United Kingdom Protocol,[22] the mean glandular dose is estimated using a polymethyl methacrylate phantom (PMMA) to simulate the breast. The exact thickness of the phantom must be accurately known. Faulkner and Cranley (1995a) found that a 2% change in phantom thickness caused variations in the estimated mean glandular dose of + 5%, - 4%. The suppliers' tolerance on a nominal thickness of PMMA is sometimes 10%, leading to a variation in mean glandular dose of +22%, -18% about that for a nominal thickness of 4 cm. Both the European and United Kingdom Protocols recommend that phantom thickness should be accurate to within 0.5 mm.

Fig. 1.14 shows the acrylic phantom used for American College of Radiology accreditation and Mammography Quality Standard Acts inspections. The phantom is approximately equivalent in X-ray absorption to a 4.2-cm thick compressed breast consisting of 50 percent glandular and 50 percent adipose tissue. The phantom includes details that range from visible to invisible on a standard mammographic film image.

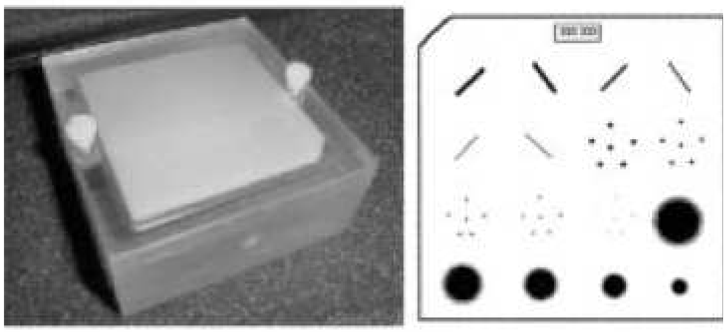

Fig. 1.14: Phantom for MQSA inspections.

The phantom has fibers with diameters of 1.56, 1.12, 0.89, 0.75, 0.54 and 0.40 mm; specks with diameters of 0.54, 0.40, 0.32, 0.24 and 0.16 mm; and masses with decreasing diameters and thickness of 2.00, 1.00, 0.75, 0.50 and 0.25 mm. The visibility of phantom details has been evaluated for screen-film and for first and secondgeneration detectors.[23] However, contrast limits guaranteed by this phantom are not enough. In fact, is difficult to enhance the contrast response on phantoms in order to simulate density tissues which have the physiological condition like those found in the breast.

These facts reveal that is necessary to develop a reliable phantom for mammography. By using a specific phantom for mammography, it is possible that the outcome contrast image would lead to a substantial improvement in the ability to identify and understand the nature of anomalous objects found in the mammogram.

The contrast detail test object developed on this work aim to offer a contrast range between 5 and 30% in digital mammography images. In addition, the uniformity and reproducibility parameters involved in their production are included. Improvements in contrast detail test objects could increase mammography image quality and even propose new quality control methods for the improvement of the mammography protocol.

CHAPTER 2

Sputtering

The following paragraphs deal with to the vapor deposition techniques used for thin films deposition, by to the sputtering technique. Sputtering system configurations and conditions used to produce thin film metallic depositions as well as their characteristics are mentioned.

2.1 Sputtering Process

A material-bombarding particle, like a single atom, ion or molecule with a relatively high potential energy can give rise to the ejection of γ electrons (secondary electrons) or other phenomenon, like breaking or rearranging chemical bonds. If the kinetic energy of the bombarding particles exceeds the binding energy of the atoms, atoms of the lattice are pushed into new position; surface migration of the atoms and surface damage may result. At energies exceeding roughly 4 H (where H = heat of sublimation of target material = binding energy of the atoms) ejection of atoms into gas phase or their dislodging starts to play an important role [5]. The new phenomenon that arises is called physical sputtering. In physical sputtering, ions rather than neutral atoms are used for bombardment, as with ions one can have the desired kinetic energy accelerating them with electrical fields. Sputtering atoms emission results as sequence of collisions that transfer momentum from bombarding particle to the emitted atom. In the Fig. 2.1 is presented a scheme of this phenomenon.

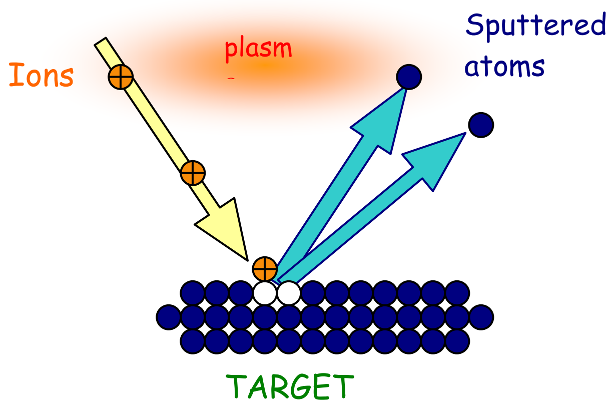

Fig. 2.1: Scheme of physical sputtering

The material changes physical state from solid to gas through a mechanical process rather than thermal or chemical process.

2.2 The self sustained glow discharge.

The main problem in order to implement a sputtering system is to design an uniform ion source over all the target surface. This can be obtained with a glow discharge. Studies and configurations have been carried out to in order to improve:

1. Increasing ion density;
2. Increasing target useful area;
3. Diminution of target heating;
4. Achieve low pressure depositions;
5. Enhance deposition on particular geometries.

If a d.c. voltage is applied between two electrodes spaced at distance *d* apart in a gas at low pressure (10^{-2} -1 *mbar),* a small current will flow. This is caused by a small number of ions and electrons, which are always present in a gas due to ionization, by cosmic radiation. On their way from the cathode to anode, the electrons make a fixed number of ionizing collisions per unit length. Each ionization process produces further electrons, while the resulting ions are accelerated toward the cathode. If the applied voltage is high enough, ions striking the cathode can eject secondary electrons from its surface. Emission ratio of secondary electrons of most material is of the order of 0.1, so several ions needs to bombard a given area of the cathode to release another secondary electron. If the supplied power is not high enough, the bombardment is concentrated near the edges of the cathode where electric field is higher. When the power supplied increases, the bombardment expands covering the entire cathode surface and a constant current is achieved.

The two processes of ionization by electron impact and secondary emission of electrons by ions, control the current *I* in the system, that is described by equation

$$I = \frac{Io\exp(\alpha d)}{1-\gamma[\exp(\alpha d)-1]} \qquad \text{(eq 2.1)}$$

where

Io : the primary electron current generated at the cathode by the external source;

α: the number of ions per unit of length produced by the electrons;

d : the spacing between the electrodes and

γ : the number of secondary electrons emitted per incident ion.

According to *Townsend criteria,* γ [exp (αd) -1] = 1 if the voltage between the electrodes is raised, the current becomes infinite, and gas break-down it is said to occur; the glow discharge ignites in self-sustained way, as the number of secondary electrons produced at the cathode is sufficient to maintain the discharge. Breakdown voltage is a function of the product of pressure *p* and electrode distance *d (Paschen's law).* Distribution of potential, field, space charge and current density in a glow discharge are visually seen as regions of varied luminosity. From a cross sectional view of a glow discharge we see of primary interest the region marked as *Crookes Dark Space* (Cathode Dark Space) (Fig. 2.2). In this region, the positive ions have accumulated and have formed the space charge.

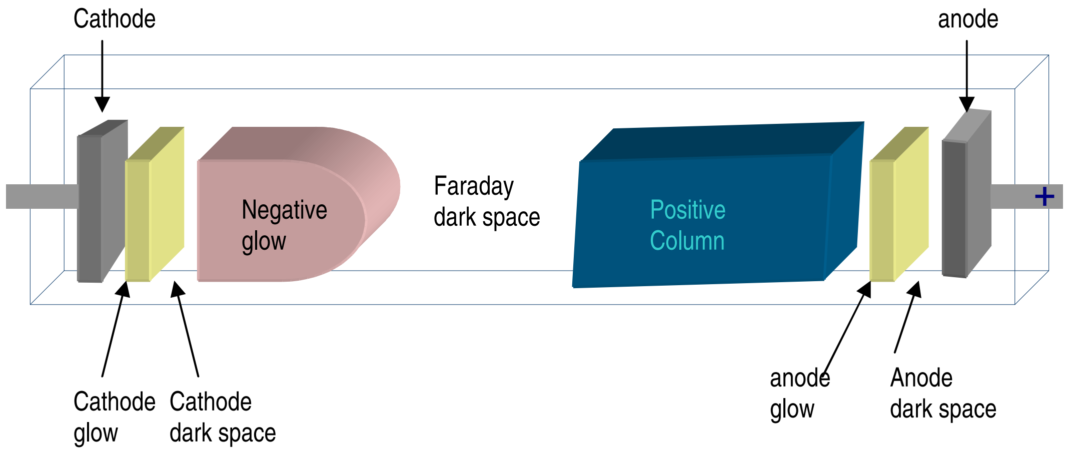

Fig. 2.2: Schematic Glow discharge view.

Its thickness is approximately the main distance traveled by an electron from the cathode before it makes an ionizing collision. Usually this distance is 5-10 times longer than the electronic mean free path *l*. The electron energies are under the maximum excitation potential which is insufficient to ionize gas molecules, so that no visible light is emitted. Electrons that leave the cathode with energy of the order of 1 eV are accelerated sufficiently to ionizing energies in region called *Aston's dark space.* The luminous region that is most close to the cathode is *the cathode glow* where the electrons reach energies corresponding to the ionization potential. When the electrons reach the edge of the *negative glow,* they begin to produce significant numbers of ion-electron pairs. The number of slow electrons (i.e. those produced by an ionizing collision) has become very large. The energy they possess is enough to cause only excitation and can not produce new ionization. Excitations caused by slow electrons are the reason of the appearance of the negative glow. In *Faraday dark space* the electrons have insufficient energy to cause either ionization or excitation, consequently is a dark space. Faraday dark space and the positive column are nearly field-free regions with nearly equivalent number of ions and electrons. For glow discharges applied as sputtering sources, the positive column and the Faraday dark space usually do not exist, as the electrode separation needs to be small and the anode is located in the negative glow.

2.3 Sputtering configurations

Sputtering is a technique by which atoms and ions of argon or other gases from plasma bombard a target there by knocking atoms off of the target. These material atoms travel to a substrate where they are deposited and form a thin film. The simplest configuration of a sputtering source is shown in Fig. 2.3. Diode sputtering configuration consists in two electrodes placed in a vacuum chamber.

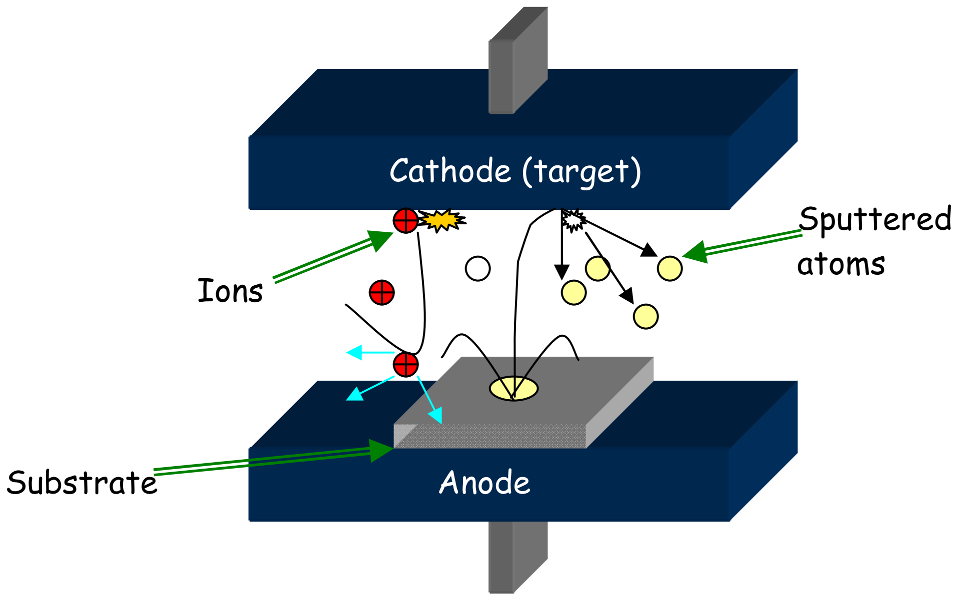

Fig. 2.3: Diode Sputtering.

An anomalous glow discharge between 2 electrodes is created if d.c voltage of ca. 500 V is applied. The substrate were the film is deposited is placed on the anode, while the target that will be sputtered represents the cathode (the negative electrode). High or ultra high vacuum is necessary to achieve thin film purity. After evacuation to high vacuum or ultra high vacuum (UHV) the chamber is filled with the sputtering gas, usually argon, at pressure of 10^{-2} or 10^{-1} mbar. Applying a d.c. voltage of ca 1-5 kV between cathodes will create a glow discharge that will ionize the argon gas. Positive ions of argon will be accelerated towards the cathode and due to their high kinetic energy will eject atoms from the target surface. The ejected atoms have energies on the range of several eV. They will diffuse in chamber till they condense on the surface of substrate. The high kinetic energy of sputtered atoms leads to a better adhesion and higher density of sputtered thin film.

The number of ejected atoms per incident ion is called sputtering yield. The minimum ion energy required to dislodge target atoms is called *sputtering threshold.* The sputtering yield increases first exponentially above the sputtering threshold (10-30 eV), then linearly, then less linearly till it approaches a flat maximum at energies of 10 keV. With further increasing of ion energy, an ion implantation effect takes place and the sputtering yield decreases.

The sputtering yield depends on the following parameters:

- *Bombarding ion energy* influence the sputtering yield as explained above.
- *The atomic number of the collision atoms*: The masses of target atoms influence the energy transfer following the expression:

$$E = \frac{4mM}{(m+M)^2} \qquad \text{(eq. 2.2)}$$

where m= mass of target atom, M= mass of ion

That means that for a high sputtering yield the mass of target atom should be not very different from the mass of bombarding ion.

- The experiment clearly shows that *noble gas* ions give the highest sputtering yield. Since this since inert gases are not involved in 'stealing' the electrons needed to make ionization collision near the cathode.
- *Angle of incidence of the ions:* The sputtering yields increases when less directional change of the momentum are required for ejecting atoms. This happens at more oblique incidence the sputtering yield follows the cos Ω^{-1} law and arrive a maximum for angles 45°-50° from the surface, but for values near 90° (perpendicular to the surface) the effect of ion reflection becomes dominant and sputtering yield decreases.

2.4 Magnetron Sputtering

For an effective sputtering, primary electrons must be used effectively to make sufficient ionization collisions in the vicinity of the cathode. The efficiency of the available electrons can be increased if the plasma is confined by a magnetic field parallel to the cathode surface.

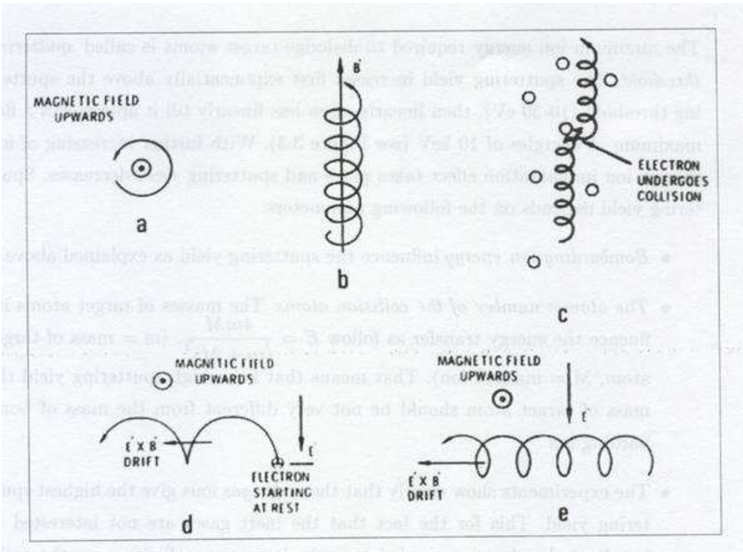

Fig. 2.4: Electron motions in static magnetic and electric fields. a) Electron motion in a magnetic field seen from up to down; b) electron drift along the magnetic field lines; c) movement of the electron when undergoes a collision; d) movement of the electron in an electro-magnetic field when there is a electric field component **E** perpendicular to **B**; e) electron has a drift speed **ExB** in an electromagnetic field.

A general rule for the shape of the magnetic field is: *Magnetic field must be born from the cathode and die onto the target.* A plasma confinement is achieved, while magnetic and/or electrostatic mirrors trap the electrons. Magnetic field traps and forces electrons to describe helical path around the lines of magnetic force (see Fig. 2.4). When ***B*** is parallel to ***E*** the particles are freely accelerated, while when there is a electric field component $E_\perp$ (Volts/cm) perpendicular to ***B***, a drift of speed $\boldsymbol{V_E}$ occurs.

$$V_E = 10^8 \frac{E_\perp}{B} = 10^8 \frac{\vec{E}\times\vec{B}}{B^2} \qquad \text{(Eq 2.3)}$$

When B is uniform and E is zero, the electrons drift along the magnetic field lines orbiting them with a cyclotron frequency ω_c and at the gyro or Larmor radius r_g.

$$\omega_c = \frac{eB}{m_e} = 1.76 \cdot 10^7 \cdot B \qquad \text{(Eq 2.4)}$$

$$r_g = \frac{V_E}{\omega_c} = \frac{m_e}{e}\left(\frac{V_E}{B}\right) = 3.37\frac{\sqrt{W_\perp}}{B} \qquad \text{(Eq 2.5)}$$

Where **B** is in Gauss and $W_\perp$ is the energy associated with the electron motion perpendicular to the field in eV.

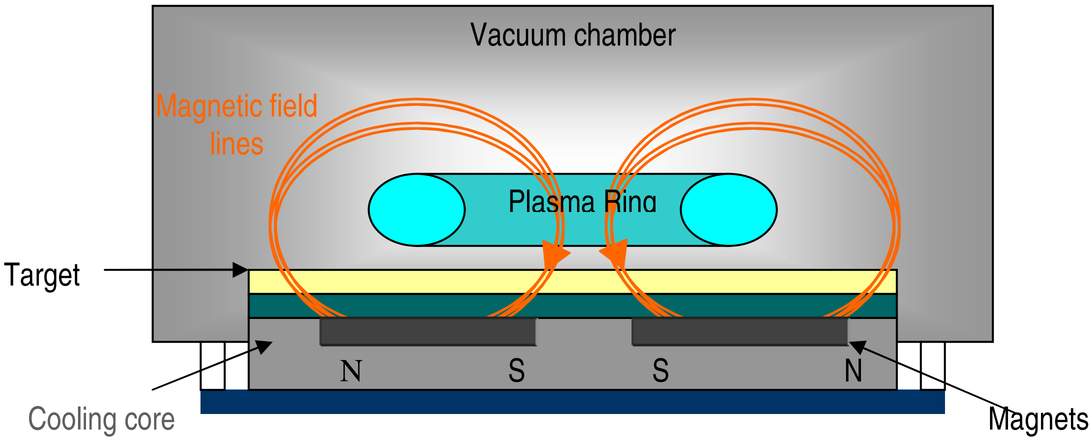

Fig. 2.5: Magnetron sputtering.

The path along which an electron travels is increased, and this increases the probability of collision. The same effects can be achieved by increasing the gas pressure. The use of a magnetic field makes possible the sputtering at lower pressure (10^{-3} mbar) if, otherwise, the pressure is not reduced, it is possible to obtain greater current for a given applied voltage. This, on the other hand, causes strong target heating making often necessary a target cooling system. As the electrons can move freely along the field lines, end losses are possible. The problem is eliminated by installing reflecting surface wings (mirrors) maintained at the cathode potential or by configuring the magnetic field lines so to intersect the cathode, as has being represented in Fig. 2.5. In order to complete the electrical circuit, the low energy electrons must be removed from the trap and migrate to the anode. It is believed that plasma oscillations assist this process. Anode placement, size and design have an important role and should take into account the poor mobility of the low-energy electrons. Proper anode placement and design can greatly reduce spurious electrical activity.

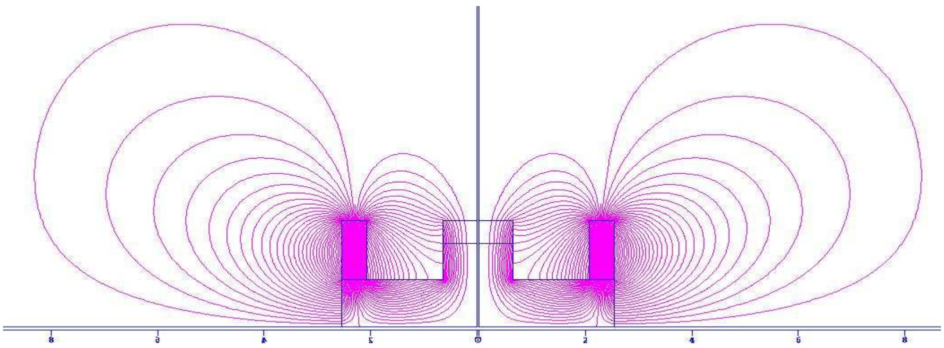

Fig. 2.6: Pandira's simulation of magnetic fields of 2" magnetron used on sputtering depositions. The magnetic field is generated by an external annular magnet and internal cylindrical one.[24]

A good design of magnetic field shape is required in order achieve the higher ionization efficiency, i.e. the highest deposition rate. The Fig. 2.6 a magnetron section with cylindrical symmetry along y-axis represents a configuration made of two magnets of equal strength in order to achieve a balanced configuration: the external annular magnet and the central cylindrical one, are placed with opposite field directions in a way that field lines start from one magnet and end on the other one.

2.5 Curve V-I

The I-V characteristic curve of magnetron reveals abundant information of ionization process in a plasma discharge. Major ionization efficiency implies minor voltage applied to achieve higher cathodic current density, in order to obtain a higher speed deposition.

There are two different models that describe dependence between current and tension applied at a sputtering source. The first – explained by Thorton – predict an exponential dependence between current and tension:

$$I = aV^{n} \qquad \text{(Eq 2.6)}$$

where the exponent *n* (that has value between 5 and 10) gives an idea of the degree of plasma ionization. Greater is this value, more efficient is the magnetic confinement.

The second one can be summarized by the following equation:

$$I = a(V - V_0)^2 \qquad \text{(Eq 2.7)}$$

where Vo is the plasma ignition potential.

CHAPTER 3

Measurement instruments

In this chapter will be described the characteristics of measurement instruments and their accuracy as well as the main operation parameters used during the analysis.

3.1 Profilometer - Thickness measure

Thickness analysis and appreciation of the uniformity of the deposition were carried out with a Profilometer *Tencor Instruments Alpha Step 200* (Fig. 3.1). The instrument consists in a diamond tip that scans the sample with a constant force. The surface roughness cause a vertical tip movement which is acquired, measured and finally registered in a plot. The measurements are done on a relatively flat sample. Determination of thin film thickness is done by measuring the step height between non deposited zone on the substrate and the grown film area. The border definition can be see on the acquired plot as well as the general shape and roughness on films surface. The instrument error on measurements was 20 nanometers, when the instrument was just bought.

Fig. 3.1: Profilmeter Tencor Instruments Alpha Step 200 used for thickness analysis.

3.2 Mammography system

The image acquisition was performed by a full-field mammography system Senogaphe 2000D. The senographe is equipped with a dual track X-ray tube and revolution ™ digital flat panel detector with a scintillator coating of cesium iodide (CsI) for conversion the X-ray to visible light. The nominal pixel pitch is 100 μm and the panel is 19x23 cm^2. Images are acquired at 14 bits giving around 8-MB images.

The X-ray images of contrast detail test object analyzed were obtain using 22 KV and 50 mAs, 71 mAs and 100 mAs.

Fig. 3.2: Mammography equipment - Image contrast measure.

3.3 Contrast Image Analysis

In order to analyze the contrast image taken from the test object, *ImageJ*[25] software is used. ImageJ is a public domain image analysis program that was developed at the National Institutes of Health.

In this work the program has been used to analyze image grey levels. The software can calculate area and pixel value statistics of user-defined selections. It can measure distances and angles; can create density histograms and line profile plots. It supports standard image processing functions such as contrast manipulation, sharpening, smoothing, edge detection and median filtering.

Equation 1.5 is used to determinate test object contrast. The digital images obtained on senographe 2000, without changes on contrast or brightness levels, were processed in order to obtain grey levels. Disks and background grey levels, disc adjacent zone, are used to make the calculations. In particular, for an specific area the program display the mean value, standard deviation, minimum and maximum value of grey levels that are proportional to the number of incident x-ray photons that arrives to detector. Circular area's have been selected. Same area for same disc diameter are used to acquire grey level so can be compared results of different objects. The Fig. 3.3 shown a front panel view of the program.

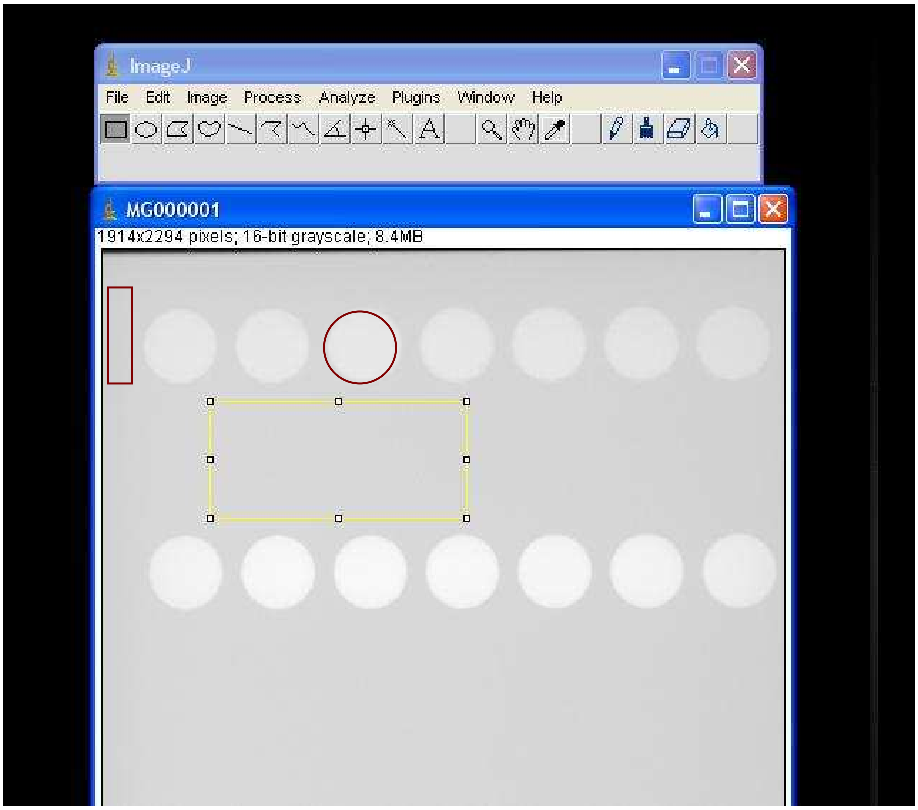

Fig. 3.3: ImageJ front panel and a contrast image view. Delimitations of measuring areas in circular and rectangular shown.

CHAPTER 4

Definition of Phantom characteristics

A brief description of the parameters to attend for phantom construction is presented. X-ray absorption characteristic of the phantoms constituents materials so as geometrical and experimental constrains are discussed. The design of the contrast detail test object, proposed in this work, is presented.

As mentioned in CHAPTER 1, PMMA have been used for phantoms preparations, offering a good approach to the breast tissues absorption. Were shown also that phantoms contain masses details imbibed to reach contrast analysis. The phantom proposed in this work has basically the same configuration. Preliminary approach is constituted of PMMA and is introduced metallic thin films, which will provide to the contrast detail test object areas with major X-ray absorption following the attenuation law described before (eq. 1.1). Selection of this metallic material and thickness of all phantom components are described on following paragraphs.

4.1 Selection of target material

Gold have been usually selected to produce major contrast areas with different shapes in contrast detail test objects. Its relatively high absorption coefficient allows one to obtain a high radiation attenuation using only few microns of material. The selection of metallic element for constructing the phantom depends on their mass attenuation coefficient and facilities of the film deposition.

4.1.1 Theoretical X-ray absorption of materials

The intensity of the x-ray transmitted is connected with the exponential of μ, the coefficient of linear absorption (from eq 1.1). μ is proportional with the density ρ of a material and so μ/ρ is constant for a given material and it is called coefficient of mass absorption and can be written in approximation as:

$$\frac{\mu}{\rho} = k\lambda^3 Z^3 \qquad \text{(Eq. 4.1)}$$

where *k* is a constant that changes along the absorption peak, λ is the wavelengths and Z is the atomic number. As expressed by the equation, X-ray absorption coefficient increases to of atomic number Z of the elements raised to the third power. Thus, the relationship between thin film thickness and X-ray absorption can be predicted, and heavy metal are a good material for producing high contrast images as required for phantom construction.

4.1.2 Theoretical calculations of X-ray attenuation in simulated phantoms.

Theoretical calculations of X-ray attenuations in simulated phantoms were carried out with PC software. In this example, sample attenuation program listing A10u8[26] was used. This program reads a spectrum file, attenuated it with a user specified number of filters and computes the tube output, mean photon energy and HVL of the filtered spectrum.

The aim of this application was to set a starting thickness values and materials for construction of a contrast detail test objects. The calculations were constrained to obtain a contrast value range from 5% to 30% evaluated over the intensity of the incident X-ray and the intensities transmitted through the filters. This result brings a theoretical thickness and material configuration for contrast detail test object construction.

Calculations were also constrained to attend X-ray dose. The simulated conditions should be almost identical to those used in mammography screening. It means that the number of photons going through the object must be controlled in the range of 1500 – 4000 mAs mm^2.

The basic configuration of simulated phantoms includes: PMMA, to simulate organic tissues attenuation and a substrate, in this case quartz, to deposit the metallic element of high X-ray attenuation, usually a heavy metal. The results of these calculations, done for several metallic elements, bring the tools to decide on the phantom constituents.

The starting parameters input were incident X-ray radiation and material thickness of phantom components. Total attenuation is calculated using incident radiation and mass absorption coefficient parameters for each phantom component. For X-ray radiation input parameters were Molybdenum tube, supply of 28 kV, molybdenum filter 0,1 mm thick and Aluminum filter 0,13 mm thick. The output obtained corresponds to the outgoing photons after going through phantom constituents.

Proposed materials and thickness, to make simulation of the attenuation of the virtual contrast detail test object, start with materials traditionally used i.e. gold. Other elements were studied considering mass coefficient absorption values and based on experimental data related to sputtering limitations.

In fact, four metallic elements were studied: Gold (Au), Tungsten (W), Niobium (Nb) and Titanium (Ti). To make the simulations, we used 4 different thickness of each metallic element. We also considered air thickness through which X-rays penetrate before arriving to the test object, established by the distance between X-ray source and the test object position. The study of all materials thickness was done systematically changing one thickness at time. The variation range of quartz substrate and PMMA thickness are shown in Table 4.1. The thicknesses of the metallic element analyzed are shown in Table 4.2.

Table 4.1: Materials thickness used in simulated phantoms for X-ray attenuation calculations.

Component	Thickness (mm)
PMMA	45
	0,5
Quartz	1,0
	1,5
	2,0
Air	640mm – (phantom thickness)

Table 4.2: Metals Thickness of simulated phantoms used in X-ray attenuation calculations.

Metal	Thickness (mm)
Gold, Tungsten, Niobium, Titanium	0,00001
	0,0001
	0,001
	0,002

Analysis was done for each metal on each thickness value as shown on Table 4.2. Contrast was calculated following equation 1.5. Background Φ_1 is the number of photons traversing phantom base material (PMMA air and quartz). Detail Φ_2 is the number of photons going trough metallic and phantom material in adjacent (to Φ_1) area.

Table 4.3 illustrates the systematic calculations done to obtain the contrast range. Tungsten and quartz thickness varies, keeping PMMA thickness, air thickness and radiation conditions identical. As a result, each row on this table represents a unique phantom configuration. The observed tendency allows knowing the general attenuation behavior for each metallic material studied. Results for titanium, niobium and gold are shown in appendix 1 as well as plotted results for different quartz thickness grouped by metallic thickness.

Table 4.3: Phantoms configurations varying tungsten and quartz thickness and their relatives contrast and outgoing photons.

Tungsten (W)

No. Exp	Anod	Volt	Filter Mo (mm)	Al (mm)	W Thickness (mm)	Air (mm)	PMMA (mm)	Quartz (mm)	Photons per mA s mm2	Contrast (%)
W1	Mo	28	0,03	0,13	0,0000	594,5	45	0,5	4286,0293	
W2	Mo	28	0,03	0,13	0,0000	594	45	1,0	3248,6042	
W3	Mo	28	0,03	0,13	0,0000	593,5	45	1,5	2487,4328	
W4	Mo	28	0,03	0,13	0,0000	593	45	2,0	1923,7172	
W5	Mo	28	0,03	0,13	0,00001	594,5	45	0,5	4280,1321	0,13759
W6	Mo	28	0,03	0,13	0,00001	594	45	1,0	3244,2917	0,13275
W7	Mo	28	0,03	0,13	0,00001	593,5	45	1,5	2484,2466	0,12809
W8	Mo	28	0,03	0,13	0,00001	593	45	2,0	1921,3422	0,12346
W9	Mo	28	0,03	0,13	0,0001	594,5	45	0,5	4227,5128	1,36528
W10	Mo	28	0,03	0,13	0,0001	594	45	1,0	3205,7677	1,31861
W11	Mo	28	0,03	0,13	0,0001	593,5	45	1,5	2455,7831	1,27238
W12	Mo	28	0,03	0,13	0,0001	593	45	2,0	1900,1129	1,22702
W13	Mo	28	0,03	0,13	0,001	594,5	45	0,50	3739,2289	12,75774
W14	Mo	28	0,03	0,13	0,001	594	45	1,00	2847,5841	12,34438
W15	Mo	28	0,03	0,13	0,001	593,5	45	1,50	2190,5759	11,93427
W16	Mo	28	0,03	0,13	0,001	593	45	2,00	1701,9234	11,52944
W17	Mo	28	0,03	0,13	0,002	594,5	45	0,50	3269,361	23,72052
W18	Mo	28	0,03	0,13	0,002	594	45	1,00	2501,5149	22,99724
W19	Mo	28	0,03	0,13	0,002	593,5	45	1,50	1933,3025	22,27720
W20	Mo	28	0,03	0,13	0,002	593	45	2,00	1508,8849	21,56410

Contrast results so obtained, with *quartz* substrate *1mm thick*, for all metallic elements studied, are shown in Fig. 4.1.

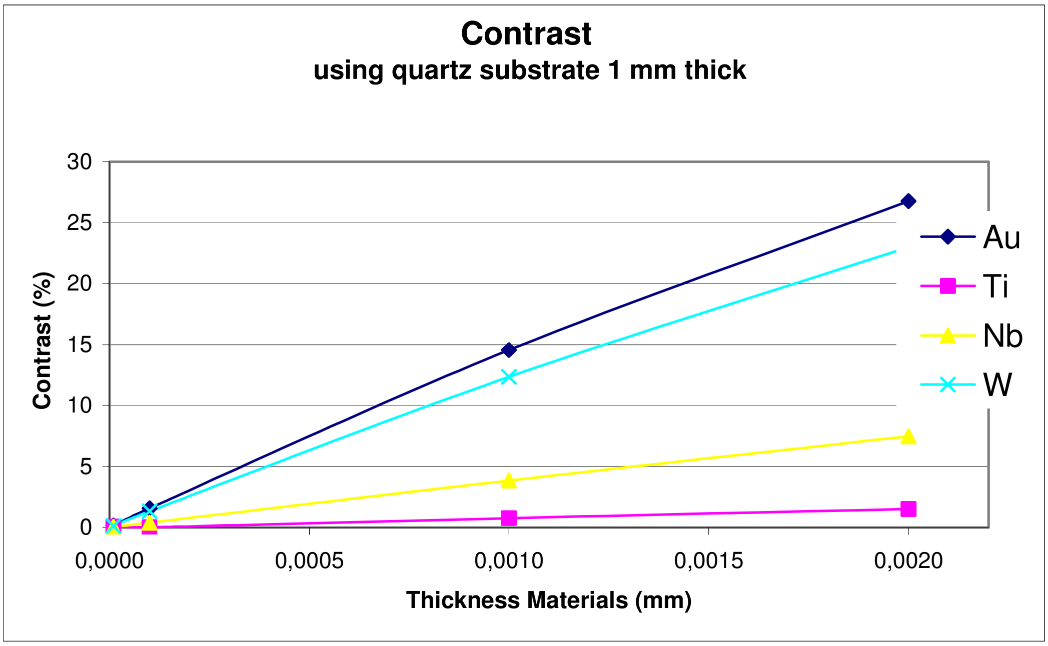

Fig. 4.1: Variation Contrast for different Au, W, Nb and Ti thickness.

The corresponding photons intensity so obtained is shown in Fig. 4.2. This plot is made in order to evaluate the radiation exposition range that should be considered during simulations. Calculations carried out varying quartz thickness, show the radiation exposure levels, which are out of the required range, as can be seen in Appendix 2.

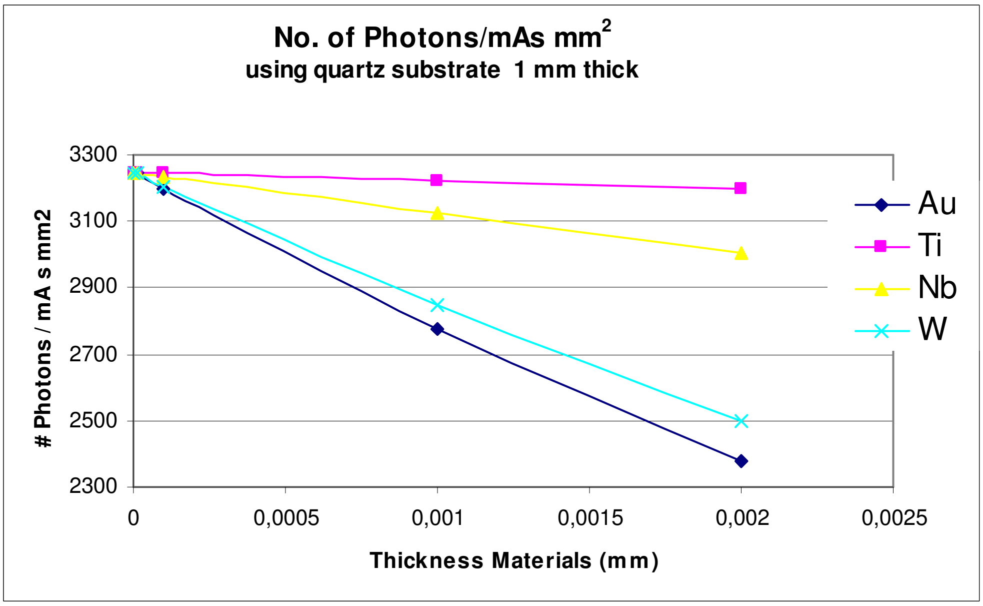

Fig. 4.2: Photons traversing different Au, W, Nb and Ti thickness

Looking the plots, gold and tungsten arises as the most convenient metallic materials for contrast detail test object construction due to their high X-ray attenuation and consequently high contrast image as required. In order to study experimental advantages and limitation sputtering related, tungsten and gold were used to make preliminary depositions.

The last criteria have considered sputtering deposition yield, availability of material and reproducibility of sputtering conditions. At this point, phantoms configuration was decided. Thickness characteristics selected are shown in Table 4.4.

Table 4.4: Thickness phantom configuration.

Material	Thickness
Quartz substrate	1 mm
PMMA	45 mm
Tungsten films	2-5 microns

4.2 Dimensions of phantom

After the simulation analysis and after the selection of materials for phantom construction, geometrical specifications of contrast details test object were projected. The design includes dimension, shape and thickness of the object, optimized to satisfy contrast range for mammography as well as sputtering experimental requirements. In particular, quartz pieces, used as substrate, must be optically flat, 1 mm thick and 50x50 mm. PMMA 50 x 50, and 45 mm thick. Tungsten thin films in the range between 2 to 8 microns were chosen.

4.2.1 Design of preliminary test object

In order to obtain contrast on different spots dimensions a 7x7 matrix of disc with different diameters deposited over optically flat quartz were designed as first approach to contrast detail test object. Disc diameter varies from 5 mm to 0,25 mm on each row as it can be seen on Fig. 4.3.

Preliminary view of the projected contrast detail test object is presented in Fig. 4.3. It can be seen, along columns same disc diameter and thickness variations. Also can be seen variation of disc diameter along the rows. Disc diameters established were 5,0 mm; 4,0 mm; 3,0 mm; 2,0 mm; 1,0 mm; 0,5 mm and 0,25 mm. Thickness variation depends on the material, in this work it will be used tungsten in the range of 2-8 microns.

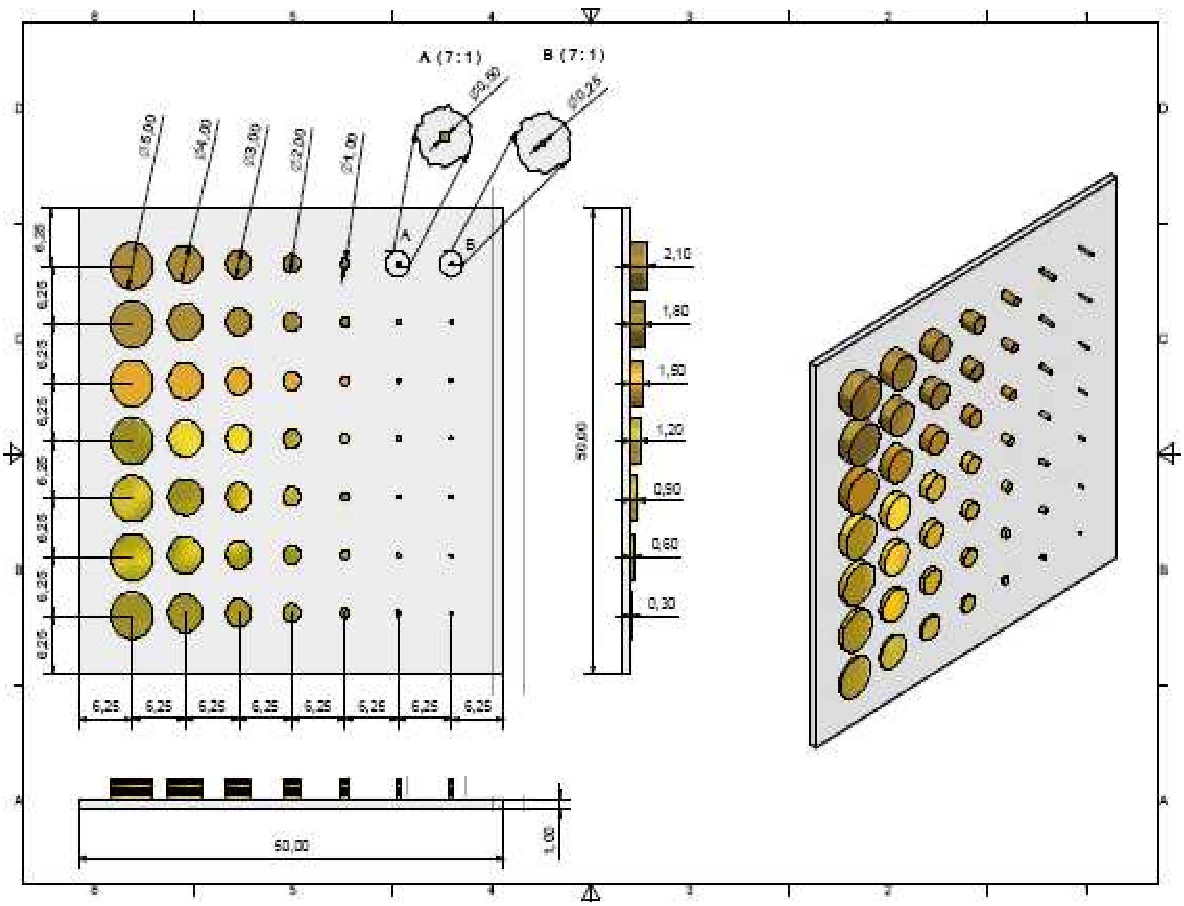

Fig. 4.3: Design of preliminary contrast detail test object

4.2.2 Mask Design

In order to deposit the tungsten, such as have been projected, was decide to use a mask to achieve the depositions according to uniformity and reproducibility constrains. This mask should cover most of the quartz substrate lying expose just the disc deposition surface. In this point, the mask material becomes an important parameter to control because its thickness influences the definition of the borders, and consequently the uniformity of the deposition.

The mask of the Fig. 4.4 was designed to be constructed on stainless steel 0,2 mm thick. The production of the mask was carried out employing a laser to cut the slide and so avoid border irregularities.

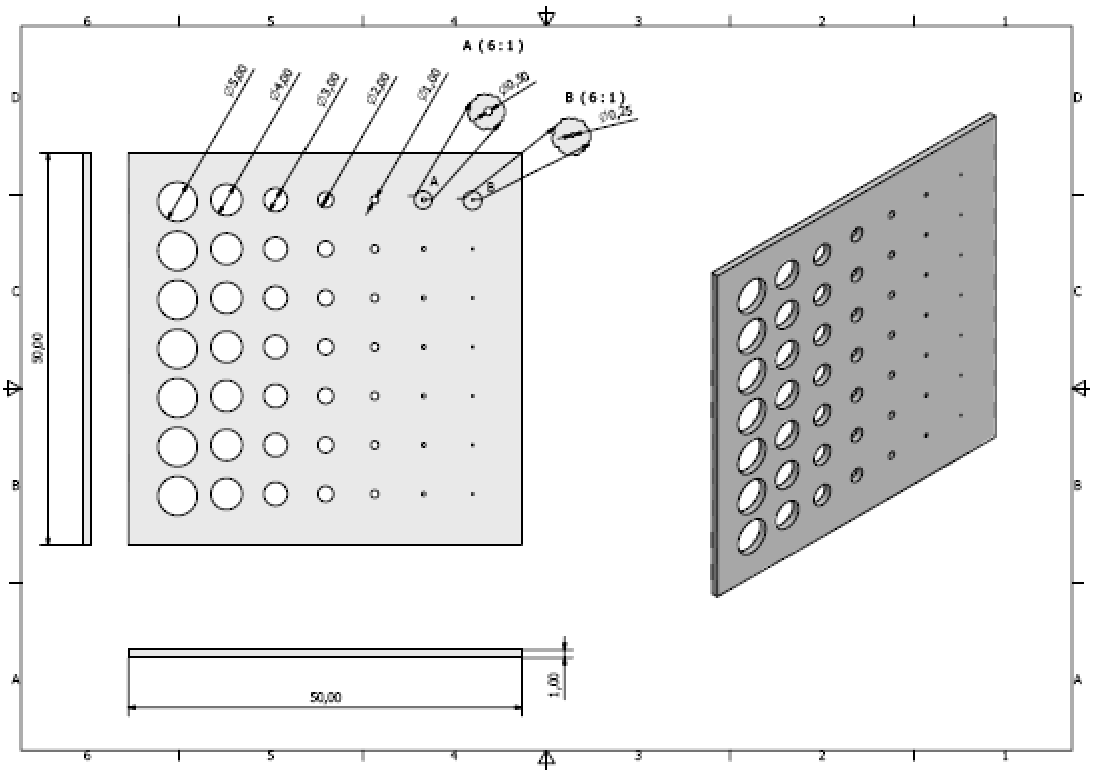

Fig. 4.4: Stainless steel mask design for sputtering depositions.

In order to assure a complete contact between mask and quartz substrate, a centering holder has been designed for firmly fixing both pieces during sputtering process. This piece has been attached to the substrate support. It is particularly useful to compensate the increasing temperature that induces a deformation mask. The *centering holder* design is shown on Fig. 4.5.

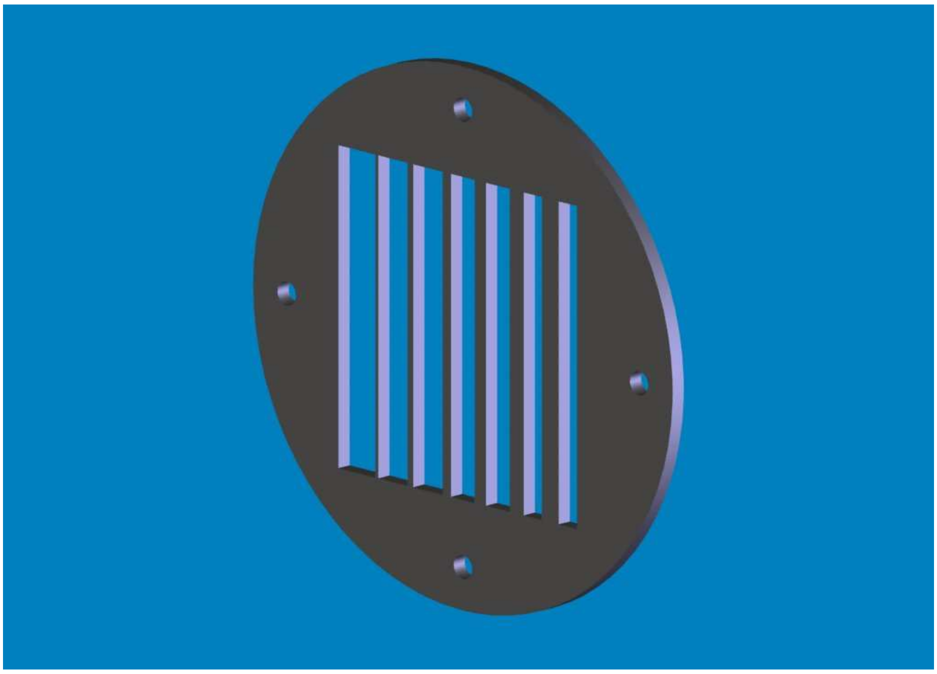

Fig. 4.5: Centering holder design.

CHAPTER 5

Deposition System Description

The sputtering systems for film deposition are described briefly. Vacuum system, cameras employed, detectors and substrate holder are included as well as parameters used during deposition together the experimental set-up.

5.1 Characteristics of sputtering systems

Thin film deposition by magnetron sputtering is a PVD process that to be performed requires a vacuum or ultra high vacuum (UHV) system. This is required to pre-clean the system that, during the deposition is, instead, at a pressure of 10^{-1} mbar of argon. A high vacuum system is mandatory and the chamber and connecting pipes inner wall cleaning is fundamental to assure low contamination. During the growing of the thin film it is necessary to avoid oxygen presence, even in ppm amount. For deposition experiment two different systems were employed: in particular, the first one is a four-chamber system, the other is composed by one chamber positioned horizontally.

During sputtering process, 2” tungsten target has been used in a magnetron source. Edax analysis were carried out over the material target reporting 93.6% (in weight) tungsten and 3.0 % Iron, 3.4 % copper. Fig. 5.1 shows several views of W target.

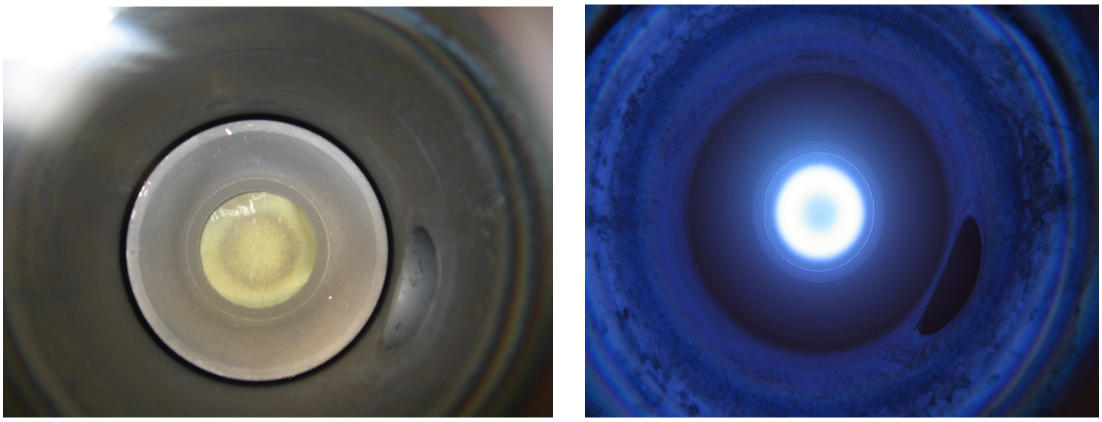

Fig. 5.1: View of Tungsten target before and during sputtering on *four chamber* system.

5.1.1 Four chamber system

The vacuum system used to carried out tungsten thin film depositions is mainly composed of four chambers stainless steel component, with internal diameters of 100 mm; chambers are placed on an imaginary square corner, connected by cross piping to the pumping units. Each chamber is connected to the central section by all metal valves to allow the possibility to separate them reducing contamination during the sputtering process. The chambers are initially evacuated by a roughing pump and, after, they reach low pressure by a turbomolecular pump. The rotary pump system is connected to central section of the cross shaped pipe through an electropneumatic CF63 gate. Between the vacuum pumps, there is a trap and a valve that closes automatically during current fails to avoid oil backstreaming. As mentioned, all parts of the vacuum system are made of stainless steel and all metal bakeable, in order to reach ultra high vacuum during the cleaning. In every chamber is mounted a magnetron sputtering source, so it is possible to carry out four independent experiments or depositions. The central cross is connected to a compact full range Bayard Alpert gauge to measure the low-pressure values that has a range between atmospheric pressure down to 10^{-9}mbar. Further a Pirani gauge and the mentioned Bayard Alpert ion gauge are employed during the sputtering process to control the pressure; an all-metal CF16 valve separates the chambers from the nitrogen line, employed to vent the system after completing the process. The system is supplied with a leak valve connected to a cylinder with the gas required, e.g. argon, during the sputtering process. The deposition occurs in argon gas at low pressure, necessary to produce convenient plasma in order to reach the desired condition for the deposition process. In particular, the depositions described in this study, were made in an environment of high purity Argon 99,9999% and a tungsten target. In Fig. 5.1 and in Fig. 5.2 the sputtering systems and the tungsten target described above, are shown.

Fig. 5.2: Four chamber sputtering system

5.1.2 Horizontal chamber system

The other sputtering chamber used to prepare tungsten thin films is of a horizontal geometry. A vacuum chamber CF150, connected to a diaphragm pump before turbomolecular pump for UHV starts operating, composes this system. Also in this case, a gate valve CF63 is placed between the referred chamber and the pumping system. Three different gauges are placed in the system measure vacuum: all range Bayard Alpert, a ion gauge and a capacitance diaphragm gauge operate during the whole process. The last one is operational during sputtering process because it gives an absolute pressure measurement, independent of gas type.

Also in this case Ar 99,9999% purity is used to feed the chamber by a mass flow controller that offers a better control of the variables for deposition reproducibility. The system includes a cooling fan to reduce chamber temperature fluctuation improving the whole process physical stability.

5.2 Optimization of magnetron sputtering parameters for W deposition

5.2.1 Deposition parameters

Tungsten thin film depositions have been done using several pressure conditions to establish the system dynamical performance and its response. Extensive experiments were done under target-substrate distance variation so that its influence on the deposition quality could be properly evaluated. One of the parameters that were considered was the time during which the deposition occurred; from the analysis of the experimental values a correlation between the pressure conditions and the best quality film adhesion on quartz substrate could be drawn as given in the following sections.

5.2.2 Tungsten characteristic curve V-I

The models that explain voltage current characteristic curve were studied in CHAPTER 1. Here we provide experimental values to obtain sputtering efficiency used as guidelines for precise operation and optimal sputtering condition.

Experimental current-voltage polarization curves have been registered for several sputtering pressures with W target using the sputtering chamber and a 2” Magnetron. Results are plotted to shown the dynamical behavior evidenced by a slope that suffers large variation when sputtering pressure is increased, e.g. by a factor of 20, as shown in Fig. 5.3. The increment in current flow can be interpreted as an enhancement on ionization process due to the abrupt increasing of electron flow between cathode and anode maintaining the same voltage (due to gas density obtained with different pressures).

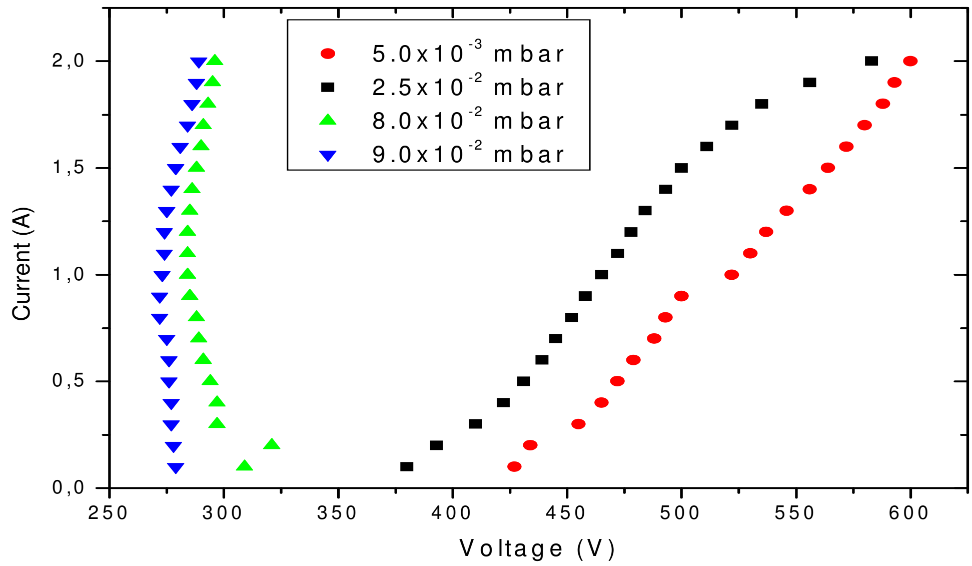

Fig. 5.3: Characteristic curve of tungsten target on 2” Magnetron.

From these results we may deduce the exponential value of equation 2.7 that expresses the relationship between voltage and current values. At a first sight, the dynamical behavior of the sputtering system suffers from non-linearity, which means only a relatively small region of values for each set of data provides acceptable values to establish the voltage exponent. The experimental results plotted as red circles, even if they have an accentuated dispersion, are the most reliable in comparison to the other three. In the case of the black diamond shape points, the curve evidences a saturation process indicating a departure from the expected physical behavior suggesting a region with values below 500 V. Departure from the expected curve, can be observed also for the other two results, from that once more, instability may be deduced suggesting that the sputtering phenomena could be considered only above the point where slope is changing from negative to positive value. In

Table 5.1 we show the voltage exponential values “n” derived from the experimental curves within the mentioned limitations.

Table 5.1: *n* values for different pressures values.

Pressure	*n* value
5,0 x10^{-3}	5,5
2,5 x10^{-2}	6,9
8,0 x 10^{-2}	11,2
9,0 x 10^{-2}	10,5

5.2.3 Sputtering Pressure

A fundamental parameter of the magnetron sputtering during tungsten deposition is the gas pressure. In fact, pressure is a critical parameter that has to be kept under strict control to avoid the forming of a residual stress during film growing, often responsible of causing the film peel off effect. Fig. 5.4 shows the evolution of a stress for a series of 150 nm thick W films as a function of sputtering gas pressure. In this case the power density at the target was fixed and the only variable was the Ar pressure supporting the previously mentioned observation.

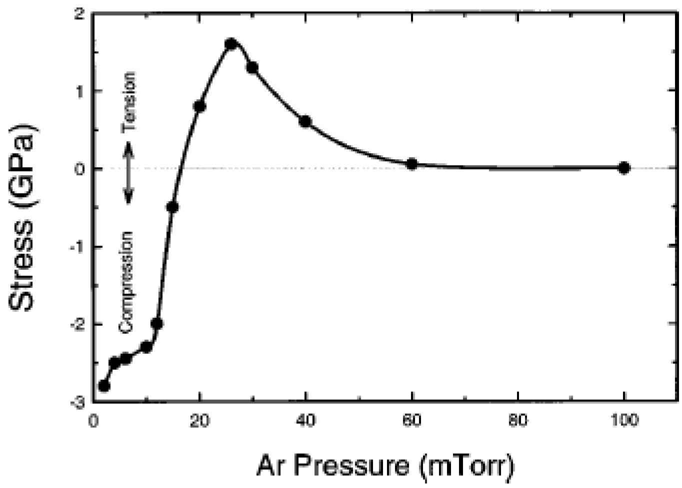

Fig. 5.4: Film stress in 150-nm-thick W films as a function of Ar sputtering gas pressure.

At the low-pressure range of 2x10^{-3} to 1.5x10^{-2} mbar, the W films are subjected to high compression stresses. As the sputtering gas pressure is increased, the stress changes from compression to tension, reaching a maximum, and with further increase the stress is gradually reversed. For pressure exceeding about $8x10^{-2}$ mbar the stress in the film is nearly zero. The compressive stress observed at low sputtering gas pressures was attributed to the bombardment of sputtered tungsten atoms and reflected Ar neutrals through a supposed atomic peening process. Conversely, the absence of energetic particles bombardments at elevated pressure scattering events leads to tensile stress. With further increasing sputtering pressure, a complex relaxation of residual stress occurs.[27]

5.2.4 Current-Voltage Optimization

Sputtering process is carried out under controlled power supplied conditions. The process is controlled in current or electric power depending on magnetron characteristics and the on system in general. Preliminary tungsten deposition was carried out to determine a set of sputtering parameters from which optimization may be derived. In table 5.2 values of experimental parameters are shown. Initially, depositions were controlled by supplied electrical power in order to establish the transferred energy during the process. Current control has been studied too, since it provides a control over the bunch of atoms deposited which in turn is proportional to the applied electrical current.

Table 5.2: parameter values for tungsten deposition.

No	Base vacuum (mbar)	Sputtering Pressure (mbar)	Voltage (V)	Current (A)	Power (Watts)	Distance (mm)	Time (min)
1	1E-5	8,9 E-2	300-450	1,3-2,0	**330**	150	60
2	8,1E-6	9,0 E-2	270-430	1,6-2,0	**700-500**	150	65
3	6,4E-6	9,0 E-2	420-300	**1,9**	850-500	150	60
4	5,8E-7	9,1 E-2	280-480	**1,9**	550-900	150	60
5	1,2E-6	9,1 E-2	290-295	**1,9**	550	70	45

Power and current values under control during the experiments are marked in bold to evidence control parameters for each deposition process done. Variations of vacuum pressure and sputtering time were done in sequence to obtain uniform depositions in concomitance to a high deposition yield. Random variations on current and voltage parameters, during the experimental sequence 1 – 4, show non-stability of the process. Experiment number 5 was carried out changing target substrate distance and deposition time.

The films 1- 4 obtained were always non-uniform and appeared under a profile-meter, with different film thickness. This result was expected due to observed variations of the applied during process. For the case deposition No.5, we introduced a change in the distance between the target and the quartz substrate. The result of the film obtained under this condition, did show uniform thickness as confirmed by measurements. Evaluating this experimental condition, it was decided to prepare thin films under current control and to diminish target substrate distance to, at least, 70 mm. A photograph of deposited substrate is shown in Fig. 5.5.

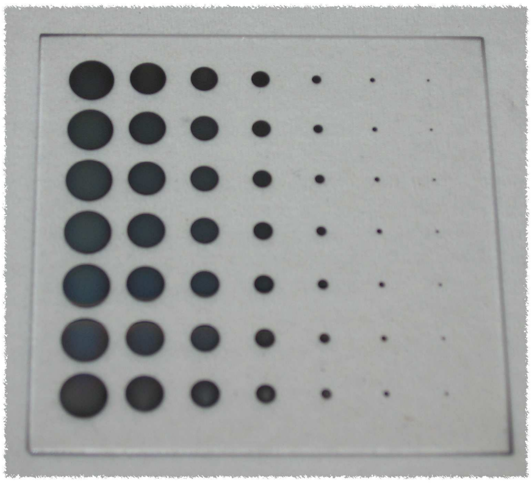

Fig. 5.5: Photography of quartz substrate with tungsten discs deposited.

5.2.5 Optimization of magnetron-substrate distance

Experimenting with target-substrate distance and deposition time interval it was possible to confirm that these parameters are correlated. The purpose of this study was to determine the existence of an agreement between deposition speed and uniformity.

In the four chambers system the sample holder is shown in Fig. 5.6 that was used in a set of experiments. In fact, in this chamber, target-substrate distance was done several steps that led to the optimized experimental condition.

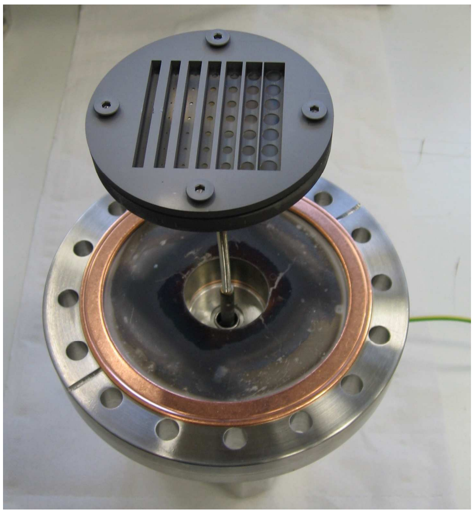

Fig. 5.6: Sampler holder used in the four-chamber system.

In the horizontal chamber system, the effect of the distance on deposition was also explored as in the previous case. However, here further consideration on the geometrical disposition was introduced to establish its property. Variations from 70mm to 30 mm target substrate distance were studied. In the case of the 70 mm target substrate distance, shown on Fig. 5.6, the result was used to set new values for the parameter under scrutiny. As we expected, high deposition rate occurs at lower separation values for target and substrate mainly due to existing correlation between deposition yield and distance. Deposition time was reduced from 60 min to 20 min obtaining similar thickness deposition therefore further experiments were set accordingly with an evident experimental advantage.

The optimization of a set of parameters, allow controlling the deposition conditions related to power supplied and therefore providing a powerful result for larger set of experiments. However, we did not overcome all related problems since several of them arise in the case of the four chamber system, related to observed random variation of magnetron current - voltage supplies; such an instability could be due to magnetron heating that often may occurs during long time sputtering process with tungsten cathode.

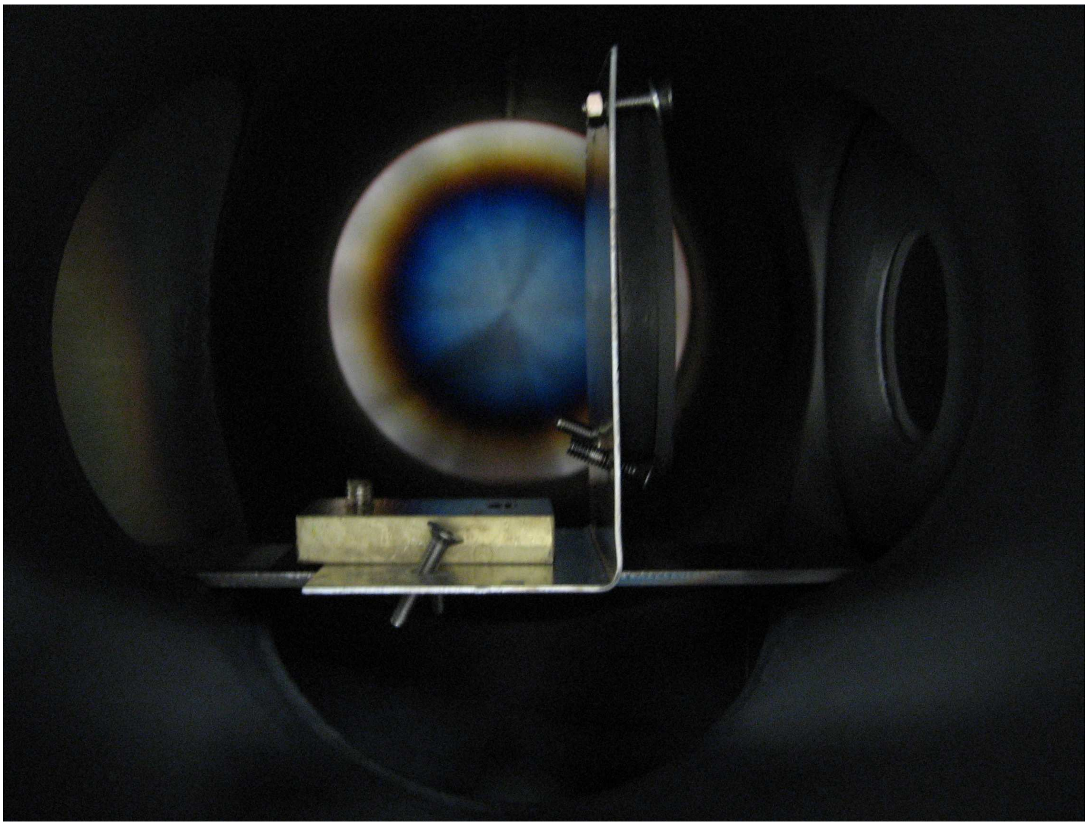

Fig. 5.7: Substrate positioned 70 mm far from tungsten target.

CHAPTER 6

Analysis of contrast detail test object

In this chapter, characterization of contrast detail test objects is reported. The achieved thickness, contrast analyses, the relative uniformity and reproducibility are discussed

6.1 Tungsten deposition

6.1.1 Thickness analysis

A test mask pattern was built in order to evaluate the thickness deposition uniformity. Early is indicated a decrease in the thickness of deposited thin films with the decreasing of discs diameter. To better illustrate results corresponding to specific disc position on quartz substrate, thickness values are represented in matrix form superposed to deposition shown in Fig. 6.1 early

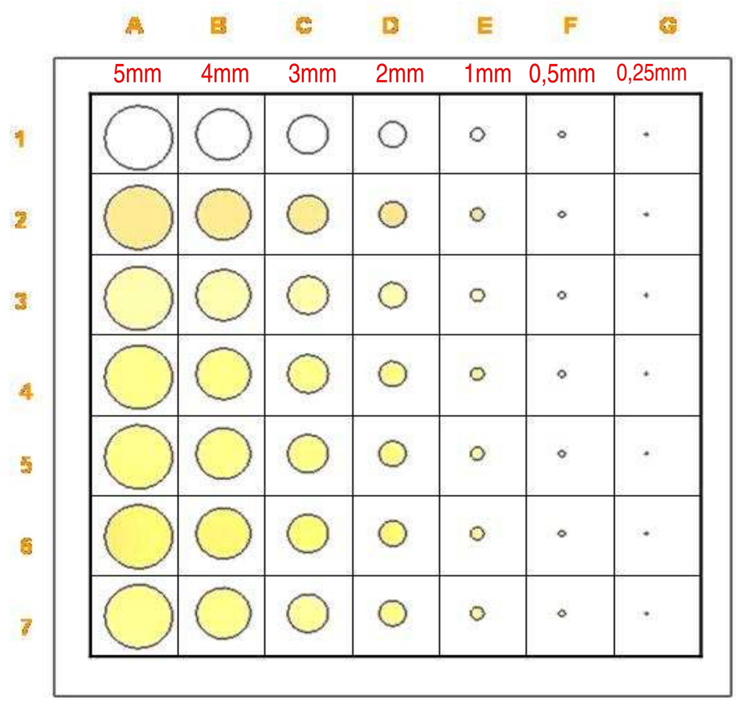

Fig. 6.1: Scheme of discs position.

A matrix table was used to tabulate the measured thickness as a function of position. It is shown in Table 6.1. Since each column represent a constant diameter sample, variation in thickness from left to right demonstrate a correlation between mask diameter and thickness. As one analyzes the data from top to bottom (i.e. constant mask diameter) you can observe that the deposition thickness is constant plus and minus 3 % from the mean value for each mask diameter.

Table 6.1: Thickness for uniform depositions.

	A	B	C	D	E	F	G
1	4.4 μm	3.24μm	3.40μm	2.48μm	2.13μm	1.23μm	0.55μm
2	5.26μm	3.70μm	3.70μm	3.00μm	2.67μm	1.45μm	0.67μm
3		3.80μm	3.83μm	3.11μm	2.68μm	1.52μm	0.75μm
4	5.15μm	3.8μm	3.81μm	3.10μm	2.71μm	1.53μm	0.74μm
5	5.16μm	3.80μm	3.83μm	3.14μm	2.68μm	1.50μm	0.69μm
6	7.15μm	3.51μm	3.63μm	3.02μm	2.60μm	1.47μm	0.69μm
7	4.34μm	3.04μm	3.09μm	2.65μm	2.30μm	1.34μm	0.63μm

As it can be observed, from Table 6.1 the maximum thickness deposited was 7.2 μm, corresponding to the 6A disc deposition. In general the thickness of the deposited material decreased as the mask diameter reduced. These results can be attributed to mask effect. The hypothesis is that mask thickness interferes with atoms displacement during sputtering process as illustrated in Fig. 6.2.

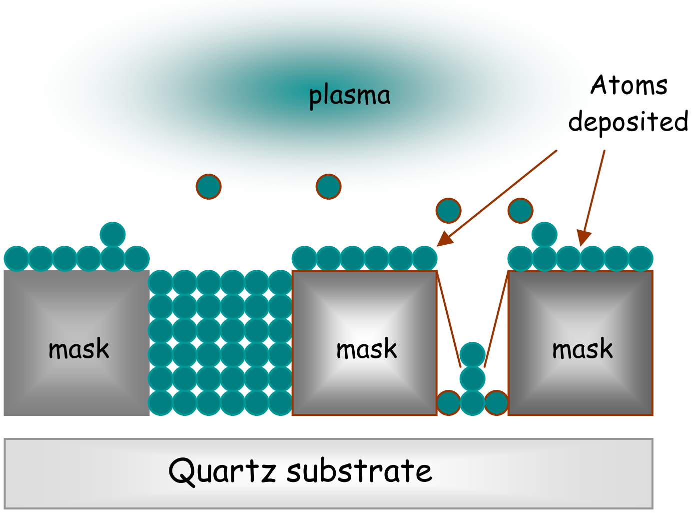

Fig. 6.2: Illustration of mask interference on sputtering deposition.

The mask shadowing effect was reduced for larger mask diameters. In contrast, for smaller diameter discs, the depositions surface had large anomalies, represented in Fig. 6.3 by a peak shape profile. These results support the hypothesis of masking effect over small diameter discs. Several experimental profile curves are illustrated for larger and smaller discs in Fig. 6.3.

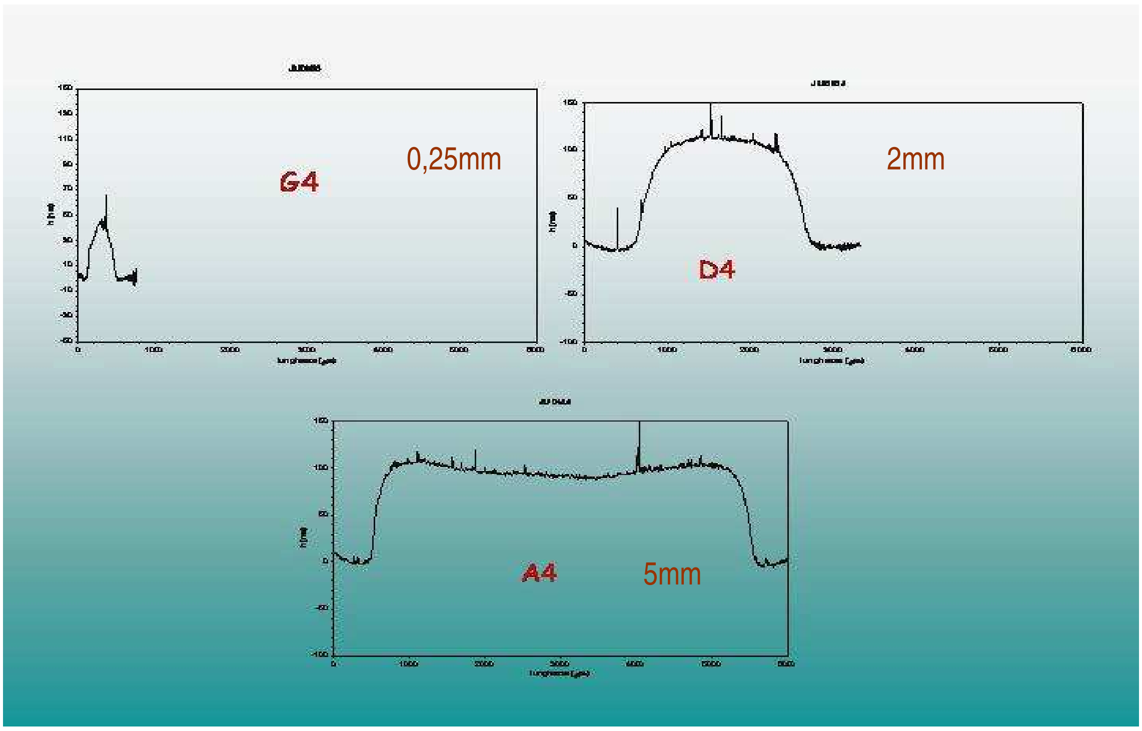

Fig. 6.3: Profiles obtained for positions A4, D4 and G4. The plots are shown in same scale to illustrate differences in thickness and diameter.

The set of results shown in Fig. 6.4 demonstrates the general trend in profiles of the deposition thickness as a function of mask diameters.

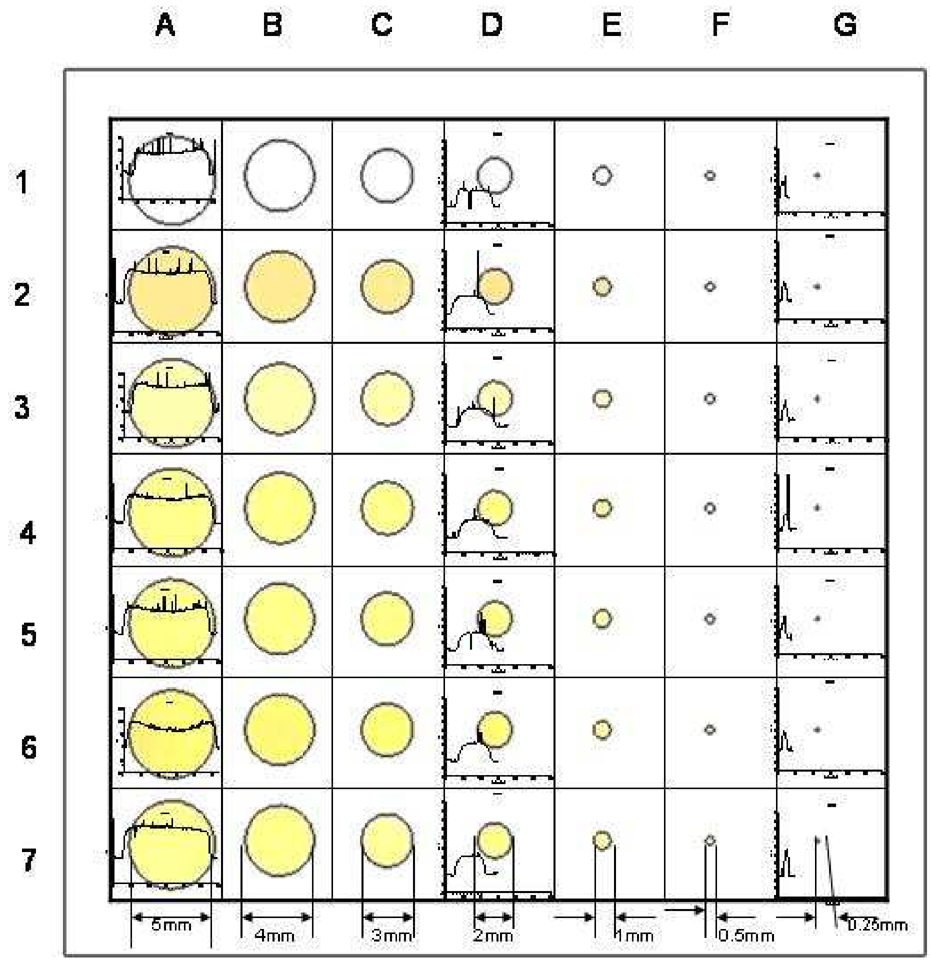

Fig. 6.4: Surface shapes obtained for larger, medium and smalls discs diameters.

6.1.2 Contrast Analysis

Contrast image of object were done to visualize the complete test object. As expected, smaller discs are invisible to human eyes, due to the low thickness and diameter. However, the border definition of the larger samples can be seen clearly and it is free of shape irregularities. Software digital analysis of contrast shows variation of gray level.

Fig. 6.5: Contrast image obtained at 50mAs, Mo22KV, Mo/Mo filter.

At the end of this series of experiments the following conclusion can be drawn:

- surface uniformity can be properly achieved using sputtering process.
- below 1 mm diameters depositions are negatively affected by mask shadowing, this results hopefully can be reduced using a mask thinner than the 0.25 mm mask used in this work.
- same range of thickness values for specific disc position were be obtained, showing a central zone of the substrate with more uniformity.
- finally, discs on the external position of Fig. 6.1 show a higher deviations in thickness values compared to those shown in the central region.

6.1.3 Reproducibility study

To study reproducibility of deposition, i.e. to obtain sputtering parameters for reproducible test objects, two sets of different types of experiments were carried out. Here the first experimental result will be presented while the other will be discus later in this work. In the first deposition three discs with thickness values in the range 1-4 μm were grown in order to establish metal thickness reproducibility. Resulting contrast image can be seen in Fig. 6.5 for which errors among three test objects were also estimated. Thickness measurements were carried out on the central discs zone, discarding the first and the last discs for each column. The results over 3 depositions in the same geometrical location of the test object are given in Table 6.2. Table 6.3contains the statistics for the samples. Values marked in bold were used for error estimation.

Table 6.2: Thickness of three different samples of five millimeters discs.

Sample 1 Thickness (μm)	Sample 2 Thickness (μm)	Sample 3 Thickness (μm)
3,5	3,5	3
3,7	4,1	3,2
3,9	**4,4**	**3,3**
3,9	**4,6**	**3,3**
3,7	**4,5**	**3**
3,3	**4,3**	**2,8**
2,88	3,6	2,2

Table 6.3: Error estimations for larger discs thickness.

	Sample 1 Thickness (μm)	Sample 2 Thickness (μm)	Sample 3 Thickness (μm)
mean	3,55429	4,13571	2,97143
std dev	0,36601	0,43274	0,38607
std error	0,13834	0,16356	0,14592
min	2,88	3,5	2,2
max	3,9	4,6	3,3

Results show a deviation of deposition thickness of the first and last rows. This is attributed to the target dimension that, in this case, was of 2” diameter. Geometrical factor influences deposition rate, being lower at external region compared to the center of the substrate. For this reason first and last rows were ignored in calculations, of mean thickness and their variations. However there may be methods to reduce this non uniformity. One potential approach is to employ a source with a target diameter in the range of 3” – 4” in diameter.

This result suggests the possibility to change also the deposition geometry, i.e. the mask design. Another alternative is to study sputtering deposition with a large magnetron target so to reduce marked variations on deposition rate.

The thickness variability for each test object was around 10%. However the resulting contrast variability was lower than 3%. A contrast image of the quartz substrate used during this experiment is shown on Fig. 6.6.

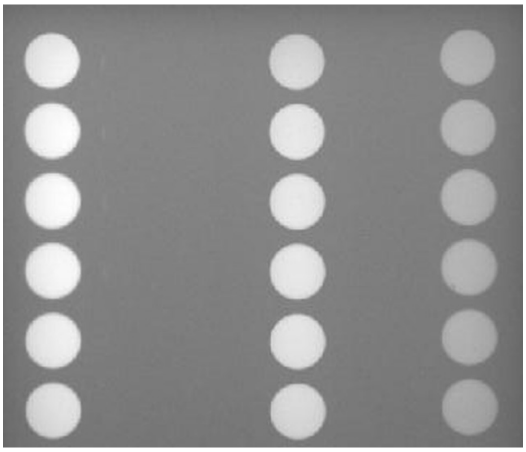

Fig. 6.6: Contrast image of different thickness tungsten deposition, decreasing from left to right, deposited on larger disc diameter.

Contrast reproducibility in this particular case was within 5%. However, this data corresponds to the larger diameter discs that give the best surface shape and border definition. Analyses over all diameter discs were done and results are given in the next chapter.

CHAPTER 7

Contrast detail test object

In this chapter, the results of several tungsten thin film thickness deposited over same substrate are presented and discussed. The techniques used to achieve and to control this thickness difference between different disc positions, are described.

7.1 Tungsten deposition with variation of the thickness

The aim of this experiment was to deposit a different thickness on the same substrate independent of the disc diameter. Previously we have discussed how the variation of thickness obtained depended on mask interference. Instead of that, thickness variation projected must be observed along of columns of discs. For this purpose two experimental methods were developed.

The first one consisted in to cover almost the complete mask, letting just one row surface uncover, in order to deposit the tungsten film one row at time. This procedure had to be done systematically, keeping the sputtering conditions almost identical for the all 7 depositions, and varying deposition time to obtain the thickness wanted. This was planned so, in order to obtain a variation of thickness along the columns and the most uniform possible along the rows due to in previous experiments, shown in chapter 6, variation of thickness were presented due to masking effect. The results obtained with this method evidence difficulty in deposition of different thickness over same substrate. The Control over all variables during 7 depositions is not so simple to achieve. Moreover, in some cases the previous deposited tungsten films were lift during the follow sputtering process done over the substrate. This method shows complexity during the process. An optimized method to obtain same objectives was proposed.

The second method studied consists in to place the substrate in a geometrical set-up, in a configuration not parallel to the target surface. This implies an inclination of the substrate respect to the target, creating different target substrate distance along of the highness of quartz substrate. The expected results for different target substrate distances must achieve different depositions thickness obtained for the same sputtering process and substrate. Theoretically, the target substrate distance is inversely proportional to the thickness deposition on sputtering process. To prove that this type of deposition can be done under control constitutes one of the objectives of this experimental section.

Finally, was deciding to carry out the experimental deposition at different thickness following the second method. In consequence, we will study the thickness dependence versus the target substrate distance for discs with the same diameter.

7.1.1 Angular positions influence

Preliminary depositions were carried out at 40, 50 and 75 degrees substrate inclination. Using these experimental results we determined that the most appropriated angle to obtain thickness deposition range with resulting contrast between 5 and 30%; this corresponds to a tungsten thickness between 2 μm and 6 μm In Fig. 7.1 we show different angular substrate positions studied.

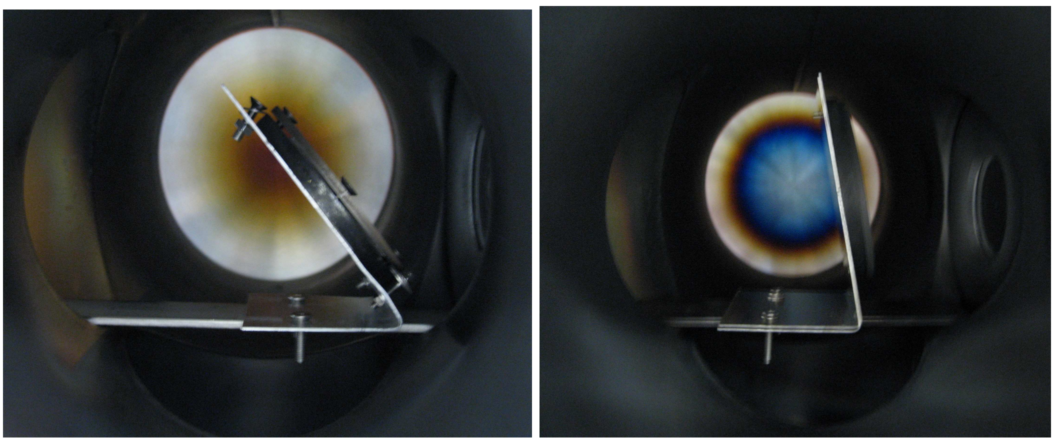

Fig. 7.1: On left 40 degrees substrate inclination, on right 70 degrees substrate inclination is given.

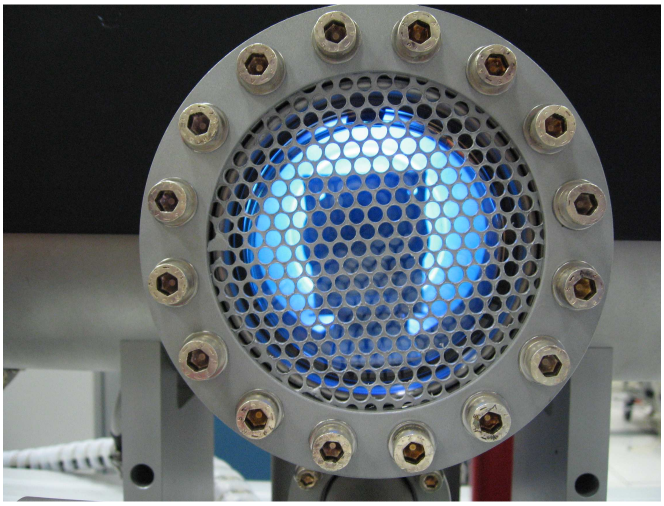

Fig. 7.2: Angled substrate view during sputtering process.

7.2 Analysis of reproducibility

One more time, contrast and thickness analysis were carried out to evaluate reproducibility of deposition and to observe its consequence reproducibility on the contrast image. Fig. 7.3 depicts the test pattern use for this portion of the work. The angle between the sputtering target and the sample was 40 degrees. The results presented in this chapter are consistent with a more extensive set of results contained in appendix 2.

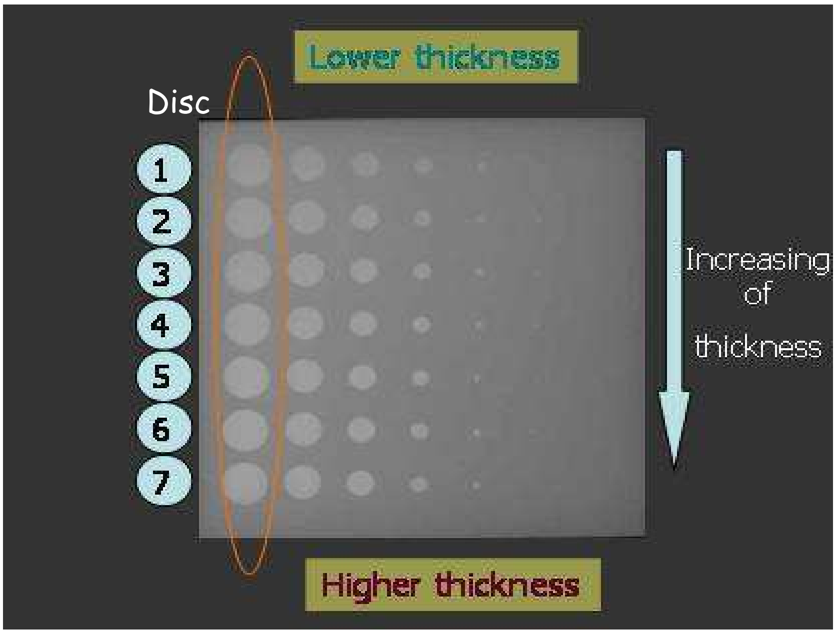

Fig. 7.3: Structure of test object analyzed on this chapter.

7.2.1 Contrast Analysis

Reproducibility of disc deposition, for each sample for a test sample is presented. Results have been grouped following disc diameter values to illustrate the general trend. The results shown in Table 7.1 are the contrast values of 2 mm disc measured for 3 different deposition cycles.

Table 7.1: Contrast reported for 2mm diameter discs in 3 different depositions.

Disc	Dep 1 (µm)	Dep 2 (µm)	Dep 3 (µm)	MEAN (µm)	STD DEV	STD ERR
1	3,05	1,574	5,555	3,39	2,01	1,16
2	5,85	4,847	7,879	6,19	1,54	0,89
3	7,94	7,967	8,816	8,24	0,50	0,29
4	9,74	9,116	9,635	9,50	0,33	0,19
5	11,32	10,553	10,054	10,64	0,64	0,37
6	12,24	12,372	9,968	11,53	1,35	0,78
7	11,18	12,104	9,079	10,79	1,55	0,89

On this set of data, we observed that the previously shown trend of diminution of the thickness with diameter. In addition it is possible to discern particularly intersecting contrast values for each disc. The mean value calculated over the set of 3 samples and their relative's errors is given Fig. 7.4.

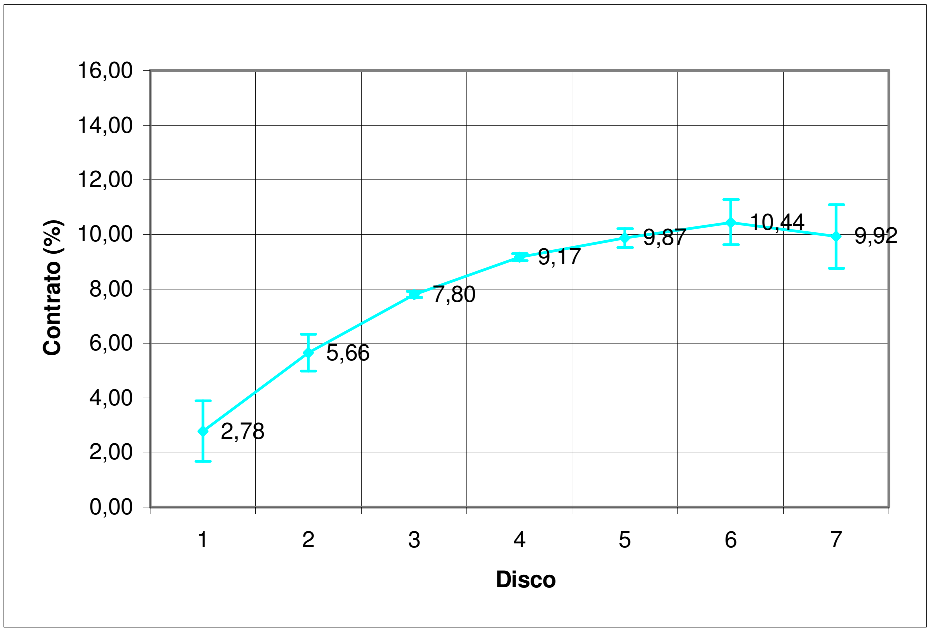

Fig. 7.4: Contrast reproducibility analysis over 2 mm diameter disc. Over each disc, was deposited different tungsten thickness.

Fig. 7.4 is a plot of the contrast values for each disc and the variance dispersion data collected show an improvement of the method. Standard deviation calculated for n=3 is always less than 2u.a., while variation is within 2%. We are aware that the determination of statistical parameters requires a larger data set to warrant an accurate phenomenological description for the group behavior. However, these experiments although limited to an essential data should contributes to understanding both the limitation and performance of the sputtering deposition technique. Several indication points to the experimentally demonstrated fact that is a versatile alternative procedure to produce test object for mammography therefore being certainly an improvement. Results also show that contrast improvement and film deposition were reproducible, since similar behavior and thickness values for specifics discs position is achieved with an error lower than 4%.

This experience also suggests that careful sputtering procedure is required emphasizing that uncontrolled phenomena occurring on first and last disk rows of the object, could be avoided also too.

Further, experimental results shown in Fig. 7.5, demonstrates the tendency of similar contrast response for almost all discs groups with same diameter value. Furthermore there is clear evidence that contrast is present with lower degree in smaller diameter discs, interpreted again, as mentioned before as caused by masking effect.

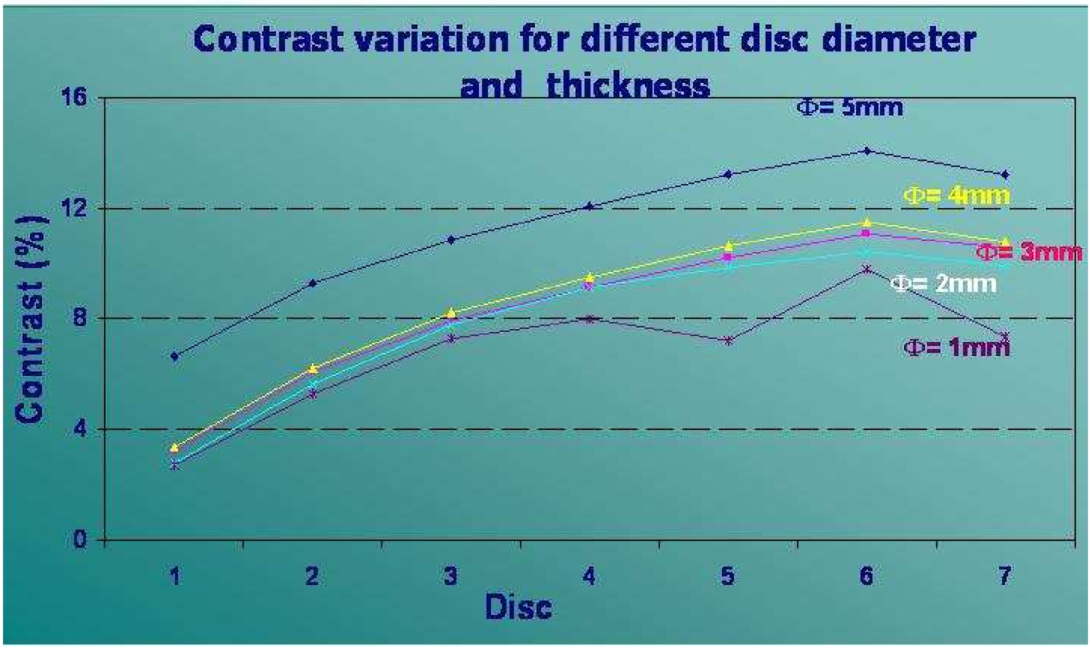

Fig. 7.5: Contrast tendency for 5-diameter disc. Over each disc, different tungsten thickness was deposited. Increasing values given from disc 1 to 7.

7.2.2 Thickness Analysis

Correlation between contrast and thickness parameter provides the parametric data required to control the test object quality. Equally important is the accuracy with which tungsten film thickness may be controlled. For 2 mm diameter disc thickness behavior can be derived from the following figure (Fig. 7.6).

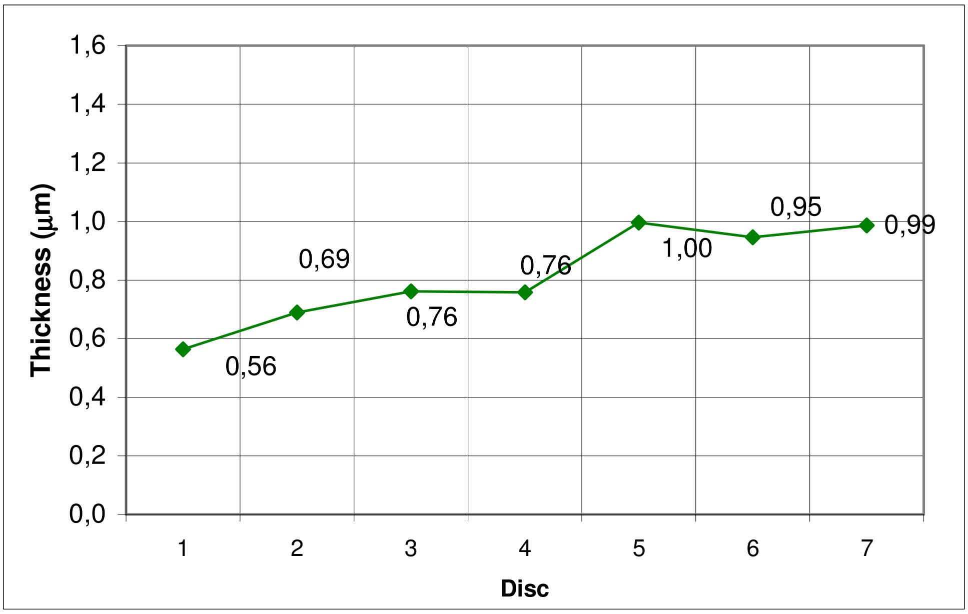

Fig. 7.6: Sputtering deposition performance for 2mm diameter disc.

The thickness range was computed to cover the whole range between 5 and 30% of nominal contrast values for the final test object. Results obtained in this experiment indicate that it is possible to produce samples with small variations in thickness and, as a consequence small contrast furthermore that it is possible to cover up to a 10% contrast range. It should be note that the lower contrast shown here is the most difficult control on test objects so far presented in literature.

Looking at thickness values and contrast results it can be appreciated that dispersion on thickness measurements is larger compared to most effective values. This effect may be related or even caused by the minor X-ray attenuation of tungsten, compared to that of gold for example that is frequently used as phantom material. In our experiments this represented an advantage since possible errors on thin film deposition thickness will not drastically influence the contrast response. This implies sputtering stability response from the contrast point of view and definitely it can be considered as a great advantage over other test object materials or depositions techniques employed so far in phantom manufacturing.

CHAPTER 8

Conclusions

- The sputtering technique as a process to deposit tungsten proposed for contrast-detail test object has proven to be an adequate manufacturing method demonstrating it can easily be used to reach the contrast efficiency in the range required by digital mammography. Furthermore that the techniques shown are a innovative improvement based on the study of reproducibility of the depositions.

- The sputtering process efficiency of metal deposition is well understood and reproducible with good uniformity for each thickness value as well as parameters stability for most of the studied experimentally important contrast region.

- It was demonstrated that tungsten target show several advantages over other more common or less expensive materials. We pointed also the advantages obtained using tungsten to measure contrast on images. Variations on thickness measurements are not evidenced in variations on the contrast. This performance can be achieved due to the tungsten x-ray absorption property, which has a slightly lower X-ray absorption compared with metals usually used in phantom production.

CHAPTER 9

Further works

1. *Development of contrast detail test object tungsten based, controlling thickness values on minor diameter discs*. For this experiment a new mask 0.1 mm thick was been designed and constructed. As shown in fig. 9.1 and 9.2, this new design consists of 6x6 matrix. Other changes have been introduced in order to obtain better contrast images of the test object.

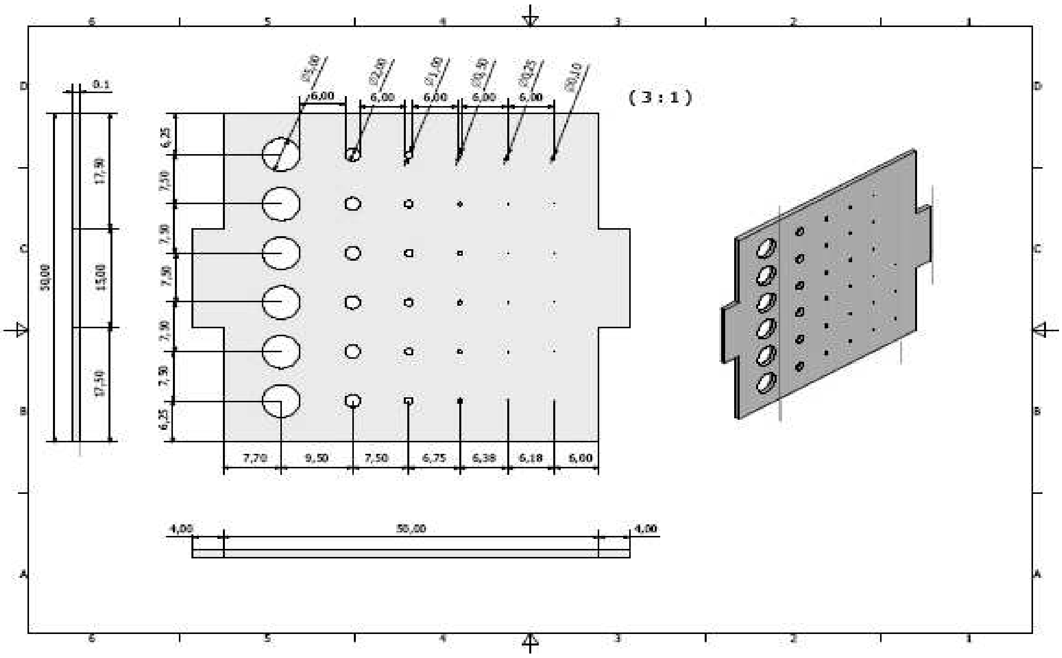

Fig. 9.1: 6x6 matrix mask design.

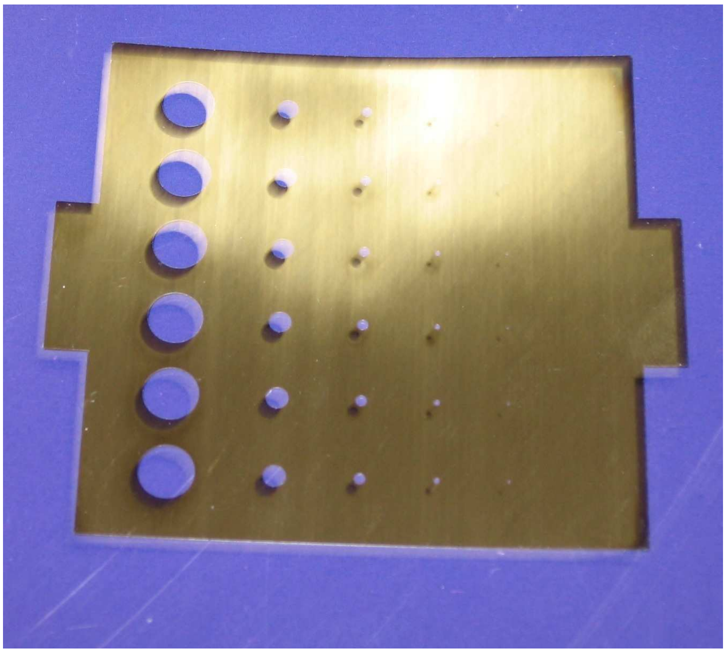

Fig. 9.2: 6x6 mask photography

2. *Enhancement of the uniformity over first and last rows.* The results suggest that larger magnetron might provide lesser end row effects. The answer suggest that a 10” magnetron be investigate.

3. Continue on studies over PVD depositions techniques to enhance precision and accuracy on tungsten depositions. A definition of a protocol to obtain tungsten film deposition in a thickness rage from 2-7mm can be proposed, after controlling the previous items related to mask effect and geometrical magnetron limitations. Employed of high precision Profilometer studies have been started. Fig.9.3 is a preliminary map scanning obtained from a row of a tungsten test object..

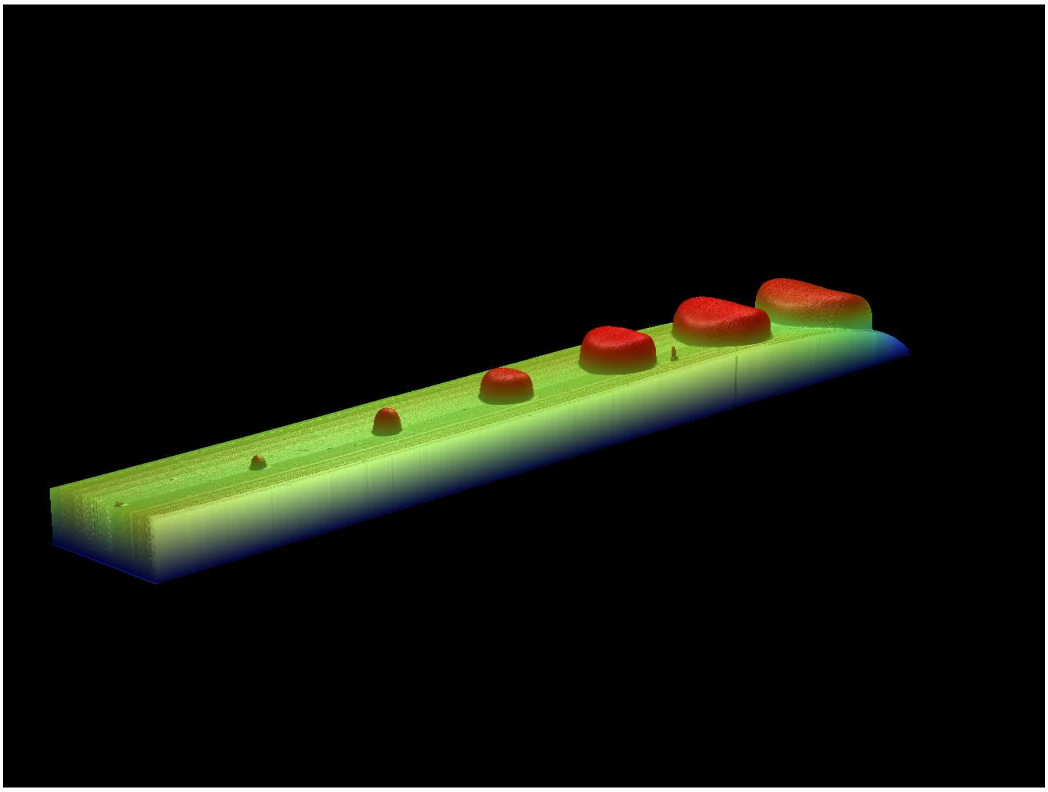

Fig. 9.3: Map scanning of tungsten deposition.

Appendix 1

Simulations results of phantom contrast for titanium, niobium and gold

Table 1. Phantoms configurations varying titanium and quartz thickness. And their relatives Contrast and outgoing Photons

Titanium (Ti)

No. Exp	Anode	Volt	Filter Mo (mm)	Al (mm)	Ti (mm)	Air (mm)	PMMA (mm)	Glass (mm)	Photons per mA s mm2	Contrast (%)
Ti1	Mo	28	0,03	0,13	0,0000	594,5	45	0,5	4286,0293	
Ti2	Mo	28	0,03	0,13	0,0000	594	45	1,0	3248,6042	
Ti3	Mo	28	0,03	0,13	0,0000	593,5	45	1,5	2487,4328	
Ti4	Mo	28	0,03	0,13	0,0000	593	45	2,0	1923,7172	
Ti5	Mo	28	0,03	0,13	0,0001	594,5	45	0,5	4282,639	0,07910
Ti6	Mo	28	0,03	0,13	0,0001	594	45	1,0	3246,1299	0,07616
Ti7	Mo	28	0,03	0,13	0,0001	593,5	45	1,5	2485,612	0,07320
Ti8	Mo	28	0,03	0,13	0,0001	593	45	2,0	1922,3632	0,07039
Ti9	Mo	28	0,03	0,13	0,00001	594,5	45	0,5	4285,6831	0,00808
Ti10	Mo	28	0,03	0,13	0,00001	594	45	1,0	3248,3565	0,00762
Ti11	Mo	28	0,03	0,13	0,00001	593,5	45	1,5	2487,2522	0,00726
Ti12	Mo	28	0,03	0,13	0,00001	593	45	2,0	1923,5817	0,00704
Ti13	Mo	28	0,03	0,13	0,001	594,5	45	0,50	4252,2854	0,78730
Ti14	Mo	28	0,03	0,13	0,001	594	45	1,00	3223,9762	0,75811
Ti15	Mo	28	0,03	0,13	0,001	593,5	45	1,50	2469,2935	0,72924
Ti16	Mo	28	0,03	0,13	0,001	593	45	2,00	1910,2315	0,70102
Ti17	Mo	28	0,03	0,13	0,002	594,5	45	0,50	4218,8447	1,56753
Ti18	Mo	28	0,03	0,13	0,002	594	45	1,00	3199,5634	1,50960
Ti19	Mo	28	0,03	0,13	0,002	593,5	45	1,50	2451,3047	1,45243
Ti20	Mo	28	0,03	0,13	0,002	593	45	2,00	1896,8553	1,39635

Table 2. Phantoms configurations varying Niobium and quartz thickness. And their relatives Contrast and outgoing Photons

Niobium (Nb)

No. Exp	Anode	Volt	Filter Mo (mm)	Al (mm)	Nb (mm)	Air (mm)	PMMA (mm)	Glass (mm)	Photons per mA s mm2	Contrast (%)
Nb1	Mo	28	0,03	0,13	0,0000	594,5	45	0,5	4286,0293	
Nb2	Mo	28	0,03	0,13	0,0000	594	45	1,0	3248,6042	
Nb3	Mo	28	0,03	0,13	0,0000	593,5	45	1,5	2487,4328	
Nb4	Mo	28	0,03	0,13	0,0000	593	45	2,0	1923,7172	
Nb5	Mo	28	0,03	0,13	0,00001	594,5	45	0,5	4284,3797	0,03849
Nb6	Mo	28	0,03	0,13	0,00001	594	45	1,0	3247,3251	0,03937
Nb7	Mo	28	0,03	0,13	0,00001	593,5	45	1,5	2486,4352	0,04010
Nb8	Mo	28	0,03	0,13	0,00001	593	45	2,0	1922,9326	0,04079
Nb9	Mo	28	0,03	0,13	0,0001	594,5	45	0,5	4269,56	0,38426
Nb10	Mo	28	0,03	0,13	0,0001	594	45	1,0	3235,8416	0,39287
Nb11	Mo	28	0,03	0,13	0,0001	593,5	45	1,5	2477,4732	0,40040
Nb12	Mo	28	0,03	0,13	0,0001	593	45	2,0	1915,8919	0,40678
Nb13	Mo	28	0,03	0,13	0,001	594,5	45	0,50	4125,2339	3,75162
Nb14	Mo	28	0,03	0,13	0,001	594	45	1,00	3123,9546	3,83702
Nb15	Mo	28	0,03	0,13	0,001	593,5	45	1,50	2390,1441	3,91121
Nb16	Mo	28	0,03	0,13	0,001	593	45	2,00	1847,2814	3,97334
Nb17	Mo	28	0,03	0,13	0,002	594,5	45	0,50	3972,6217	7,31231
Nb18	Mo	28	0,03	0,13	0,002	594	45	1,00	3005,6512	7,47869
Nb19	Mo	28	0,03	0,13	0,002	593,5	45	1,50	2297,8009	7,62360
Nb20	Mo	28	0,03	0,13	0,002	593	45	2,00	1774,7176	7,74540

Table 3. Phantoms configurations varying Gold and quartz thickness. And their relatives Contrast and outgoing Photons

Gold (Au)

No. Exp	Anode	Volt	Filter Mo (mm)	Al (mm)	Au (mm)	Air (mm)	PMMA (mm)	Glass (mm)	Photons per mA s mm2	Contrast (%)
Au1	Mo	28	0,03	0,13	0,0000	594,5	45	0,5	4286,0293	
Au2	Mo	28	0,03	0,13	0,0000	594	45	1,0	3248,6042	
Au3	Mo	28	0,03	0,13	0,0000	593,5	45	1,5	2487,4328	
Au4	Mo	28	0,03	0,13	0,0000	593	45	2,0	1923,7172	
Au5	Mo	28	0,03	0,13	0,00001	594,5	45	0,5	4278,9893	0,16425
Au6	Mo	28	0,03	0,13	0,00001	594	45	1,0	3243,4502	0,15865
Au7	Mo	28	0,03	0,13	0,00001	593,5	45	1,5	2483,6244	0,15310
Au8	Mo	28	0,03	0,13	0,00001	593	45	2,0	1920,8753	0,14773
Au9	Mo	28	0,03	0,13	0,0001	594,5	45	0,5	4216,2491	1,62808
Au10	Mo	28	0,03	0,13	0,0001	594	45	1,0	3197,4871	1,57351
Au11	Mo	28	0,03	0,13	0,0001	593,5	45	1,5	2449,6377	1,51944
Au12	Mo	28	0,03	0,13	0,0001	593	45	2,0	1895,5143	1,46607
Au13	Mo	28	0,03	0,13	0,001	594,5	45	0,50	3642,1979	15,02163
Au14	Mo	28	0,03	0,13	0,001	594	45	1,00	2775,9156	14,55051
Au15	Mo	28	0,03	0,13	0,001	593,5	45	1,50	2137,1789	14,08094
Au16	Mo	28	0,03	0,13	0,001	593	45	2,00	1661,7846	13,61596
Au17	Mo	28	0,03	0,13	0,002	594,5	45	0,50	3104,4366	27,56847
Au18	Mo	28	0,03	0,13	0,002	594	45	1,00	2379,164	26,76350
Au19	Mo	28	0,03	0,13	0,002	593,5	45	1,50	1841,7367	25,95833
Au20	Mo	28	0,03	0,13	0,002	593	45	2,00	1439,7362	25,15864

Appendix 2

Thickness and contrast variation for 5 mm disc

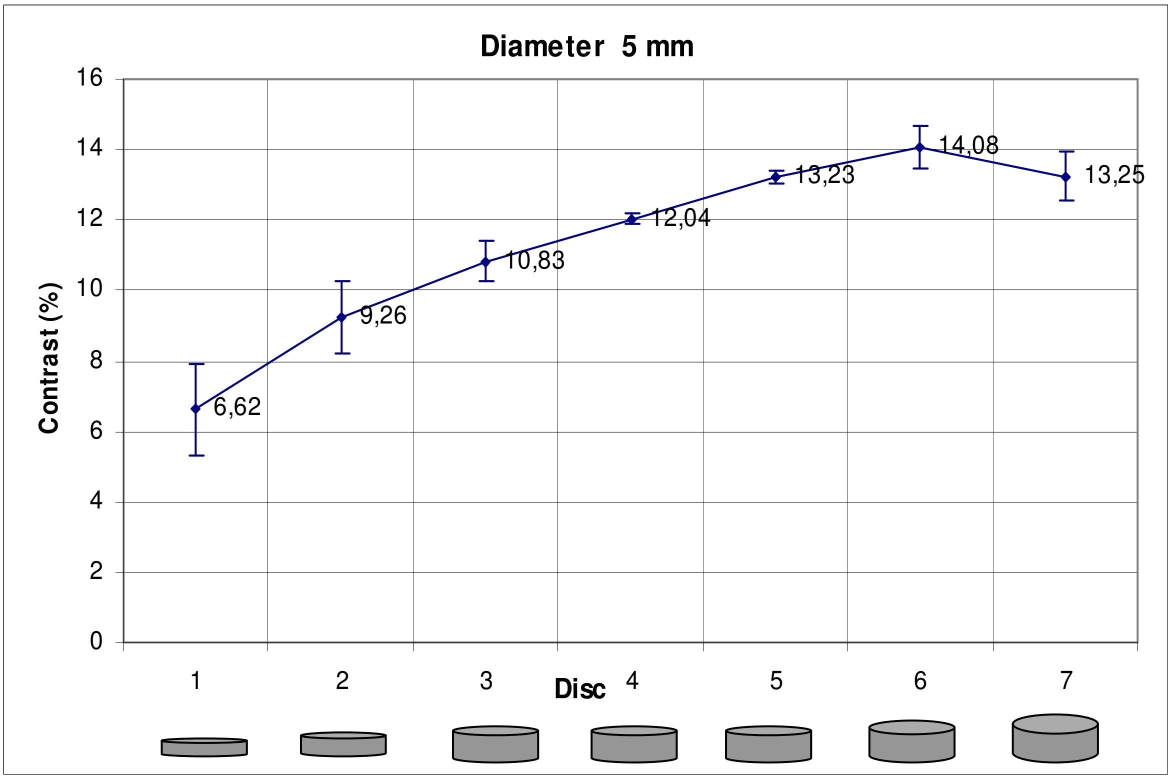

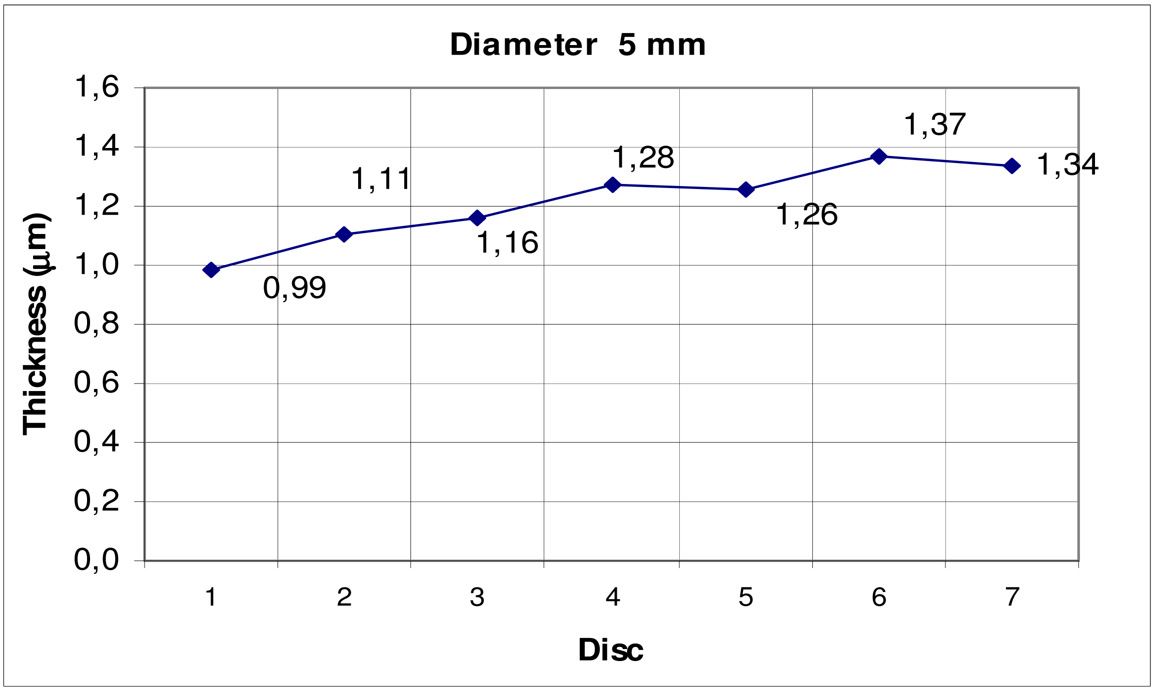

Thickness and contrast variation for 4 mm disc

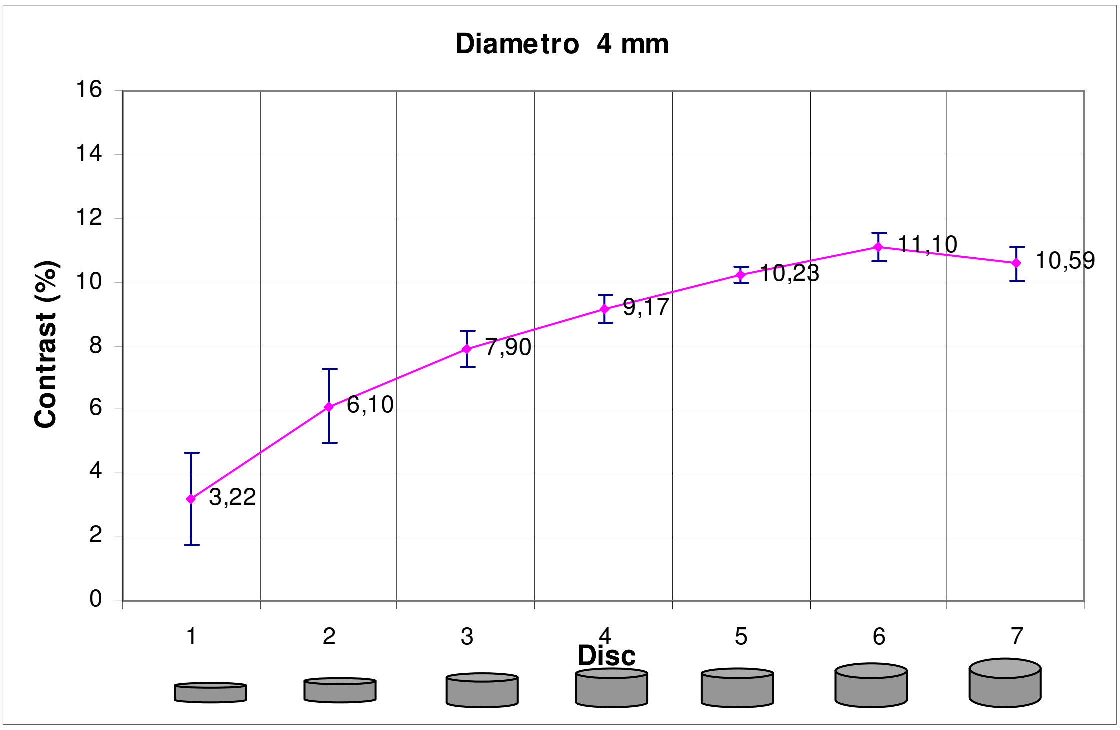

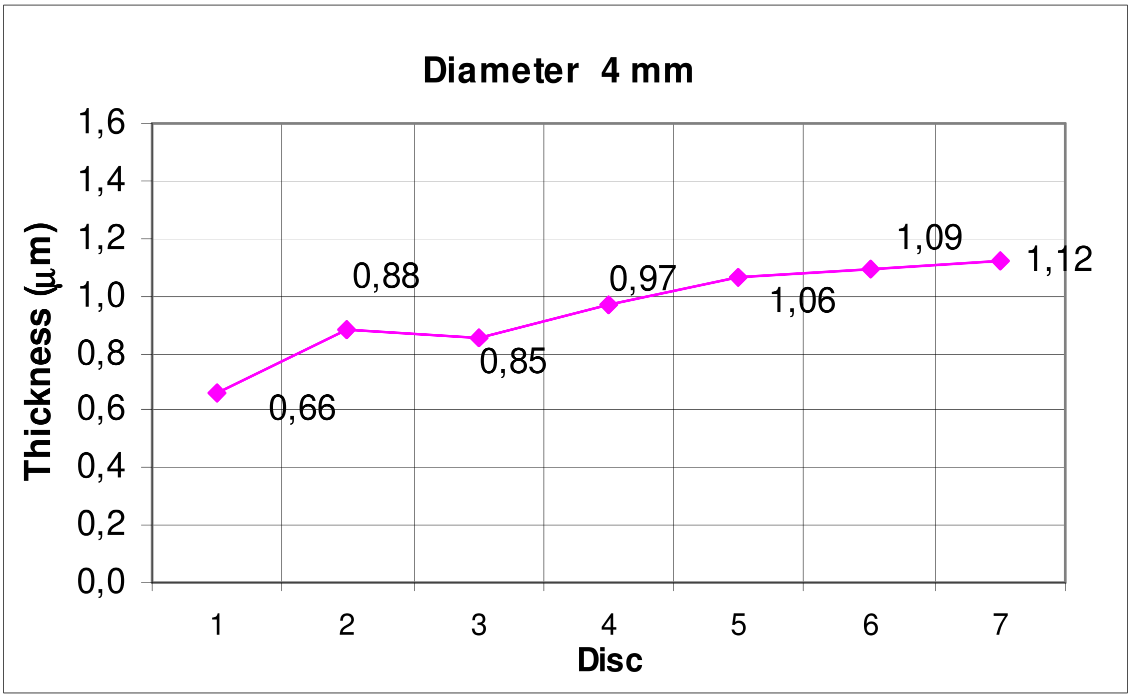

Thickness and contrast variation for 3 mm disc

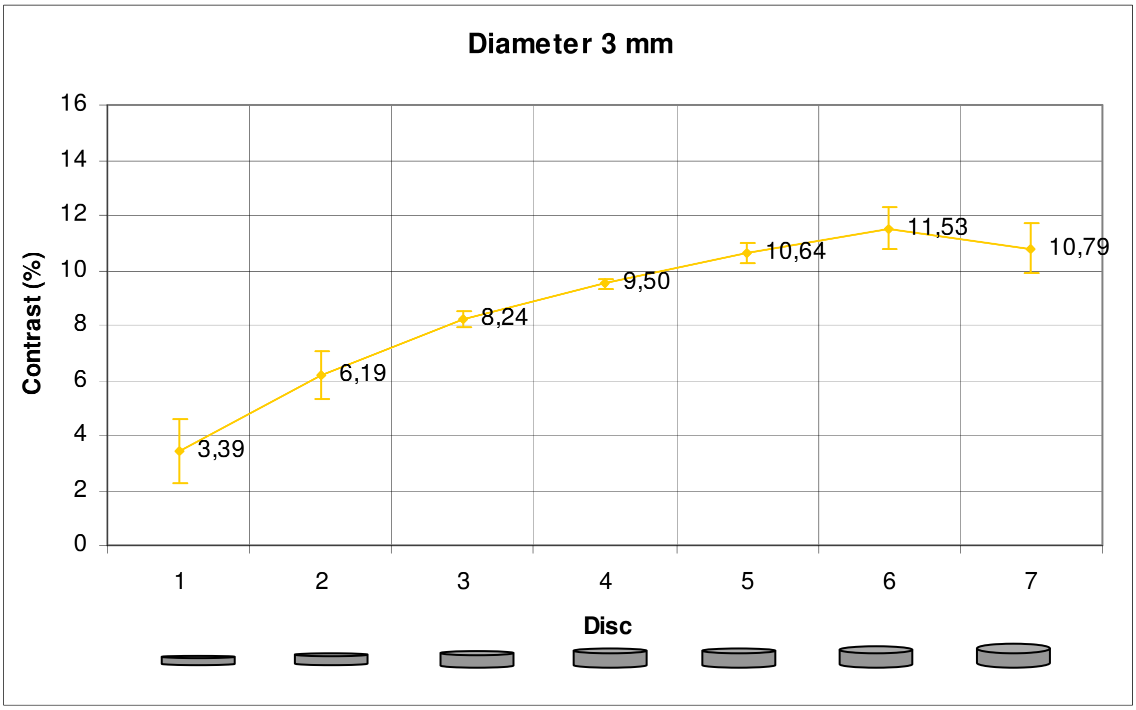

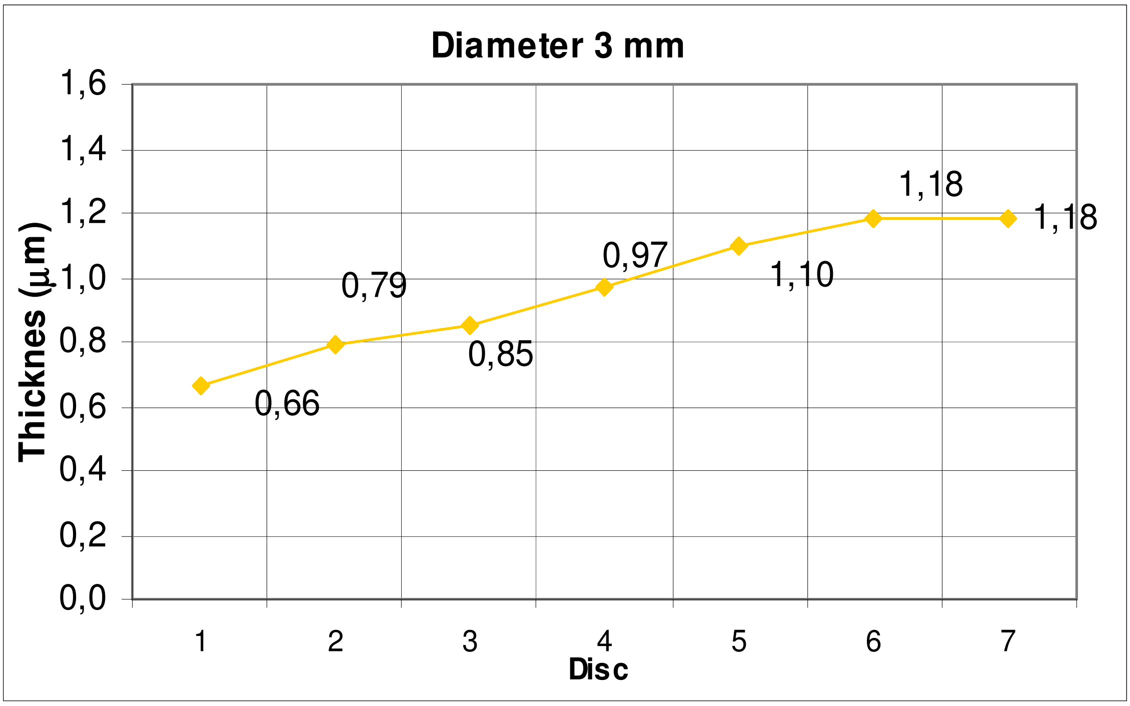

Thickness and contrast variation for 2 mm disc

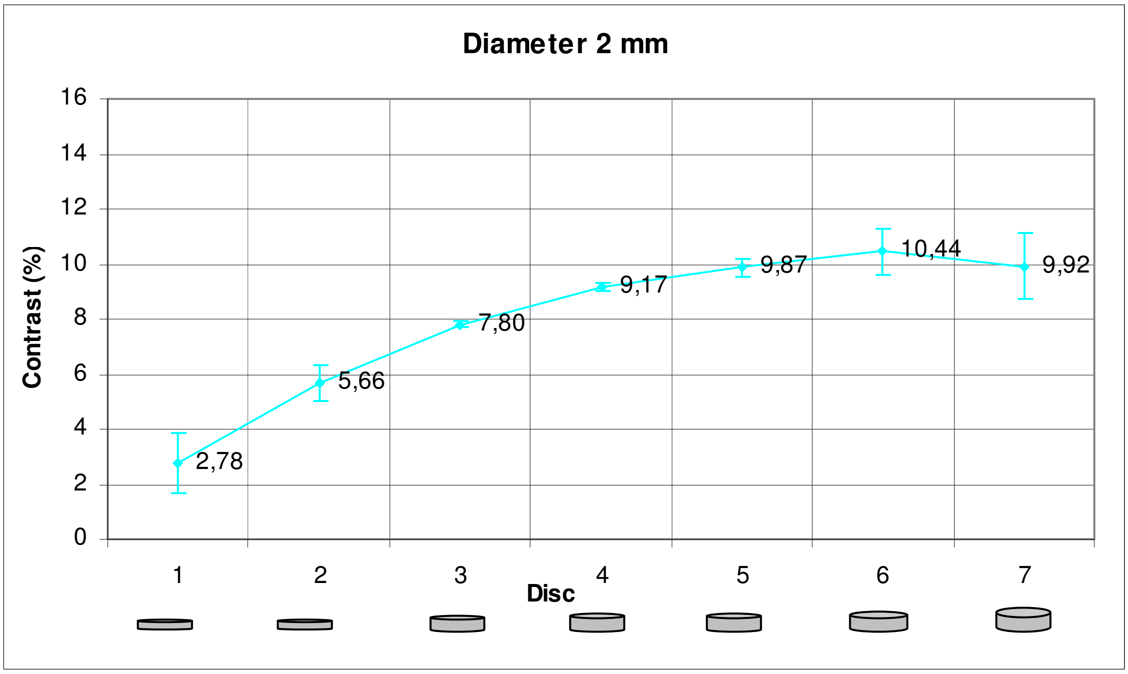

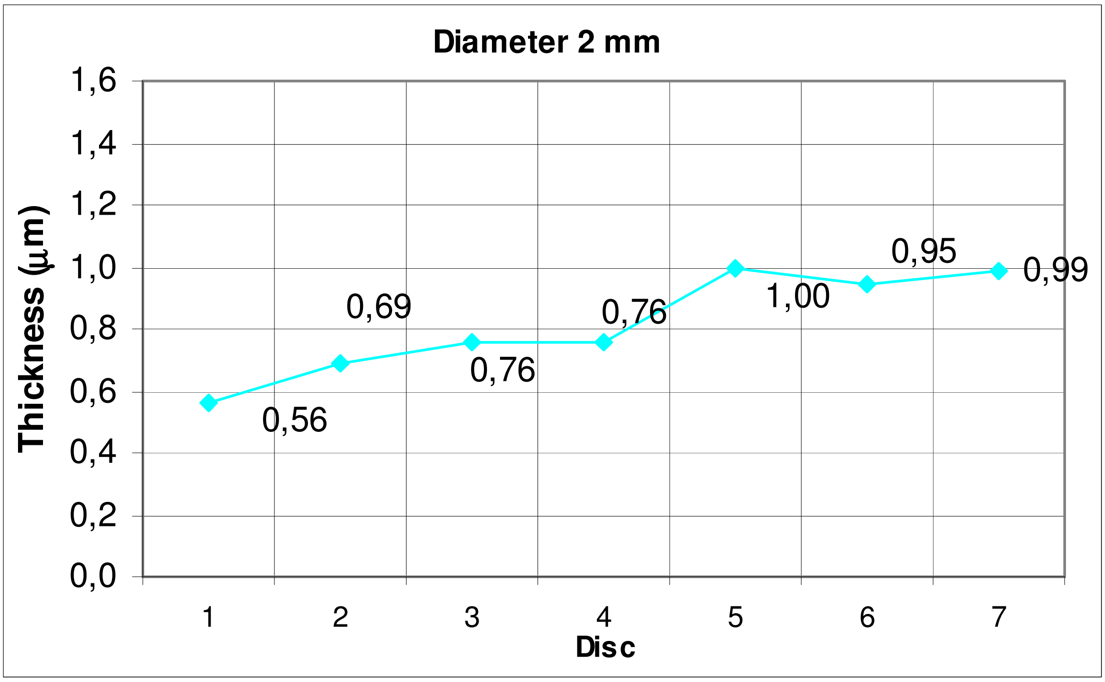

Thickness and contrast variation for 1 mm disc

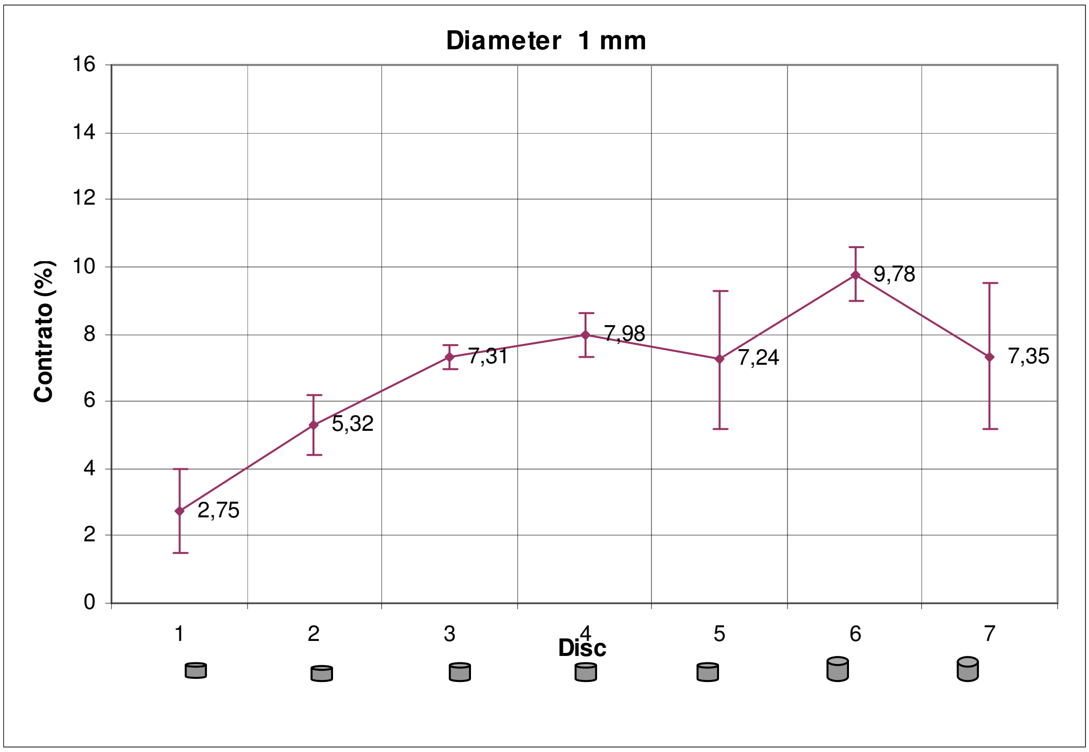

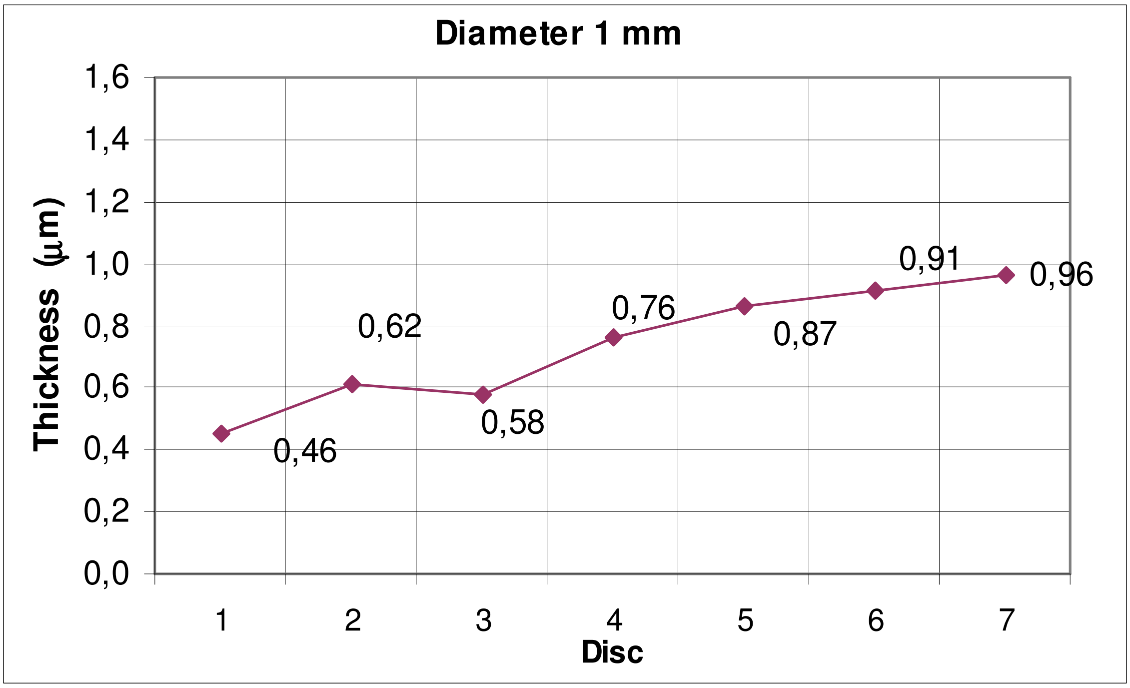

Radiation intensity of simulates phantoms for different quartz substrates thickness

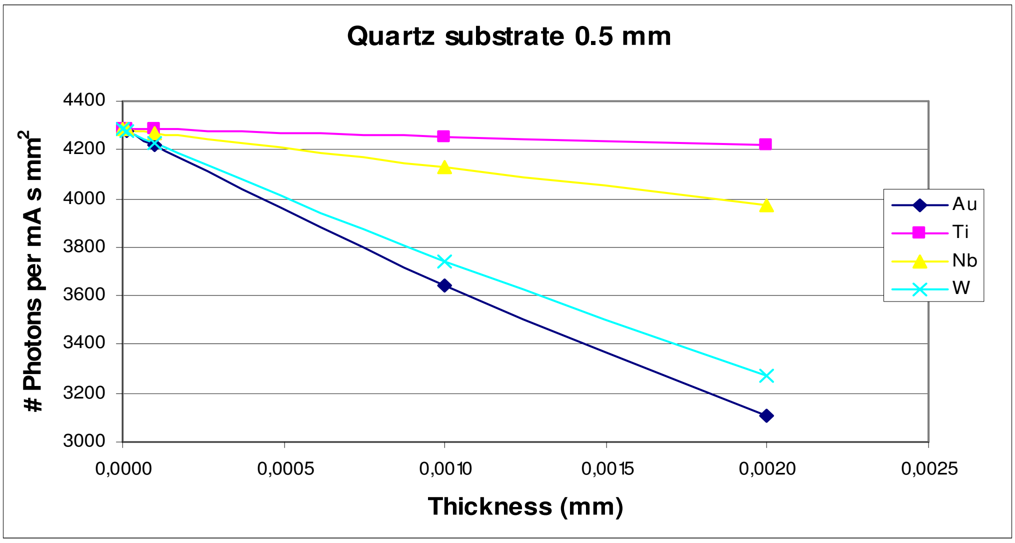

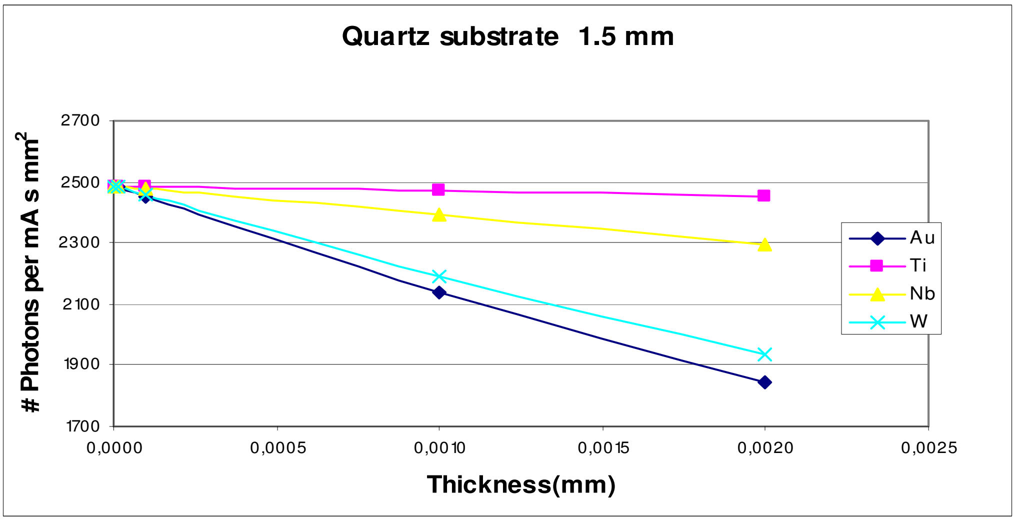

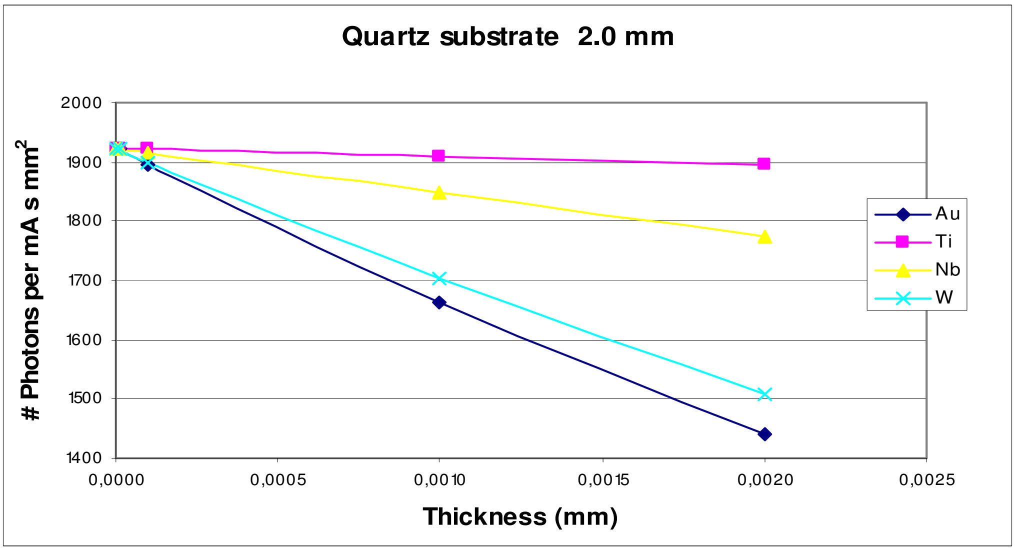

References

[1] A. Mavroforoua, D. Mavrophorosb and E. Michalodimitrakis. Screening mammography, public perceptions, and medical liability. European Journal of Radiology Volume 57, Issue 3 ,(2006), 428-435.

[2] G.K. Loudos, N.D. Giokaris, K. Mainta, N. Sakelios, E. Stiliaris, A. Karabarbounis, C.N. Papanicolas, V. Spanoudaki , K.S. Nikita, N.K. Uzunoglu, S.C. Archimandritis, A.D. Varvarigou, K.N. Stefanis, S. Majewski, A. Weisenberger, R. Pani, D. Maintas. High-resolution and high-sensitivity SPECT imaging of breast phantoms. Nuclear Instruments and Methods in Physics Research A 527 (2004) 97–1.

[3] C.J. Martin, P.F. Sharp, D.G. Sutton. Balancing patient dose and image quality. Applied Radiation and Isotopes 50 (1999) 1-19.

[4] A. Larry DeWerda, Louis K. Wagner. Characteristics of radiation detectors for diagnostic radiology Applied Radiation and Isotopes 50 (1999) 125±136.

[5] K. Geleijns, W. Teeuwisse and W. Veldkamp. The Dutch demonstration project for patient dosimetry in diagnostic radiology.

[6] G. C. E. Burger. Phantom tests with X-rays,. Philips Tech. Rev. 11, (1950) 291±298.

[7] Boone John M. Glandular breast dose for monoenergetic and high- energy X-ray beams: Monte Carlo Assesment. Radiology volume 213 no. 1. (1999).

[8] C. Di Maggio, M. Gambaccini, G. Gennaro, P. Balzelli, A. Taibi, R. Chersevani, S. Limoneto, V. Rossetti, D. Origgi, S. Vigorito, G. Contento, L. Angelici, S. Maggi. Mammografia digitale: Controllo de qualità e della dose. Reposrt n. 1 del gruppo di lavoro AIFM sulla mammografia digitale. La Radiologia Medica. 107. 459-473, 2004. Edizzioni Minerva Medica- Torino.

[9] R. V. Stuart. Vacuum Technologies, thin films and sputtering. Academic Press 1983. pp. 137-148.

[10] Woodard, H. Q., White, D. R., The composition of body tissues. British journal of Radiology 59, 1209-1219.

[11] Andrew Smith. Fundamentals of Digital Mammography: Physics, technology and practical considerations. Radiology management september/october 2003.

[12] M.Karlsson, K. Nygren, G. Wickman, G.Hettinger. Absorbed dose in mammary radiography. Acta Radiologica Therapy Physics and Biology 15, (1976) 252±258.

[13] ICRP International Commission on Radiological Protection, 1987. Statement from the 1987. Como meeting of the ICRP. ICRP Publication 52, Annals of the ICRP 17(4).

[14] D.R. Dance, C.L. Skinner , G. Alm Carlsson. Breast dosimetry. Applied Radiation and Isotopes 50 (1999) 185±203.

15 Radiology management, September October 2003.

16 Fundamentals of Digital Mammography: Physics, Technology and Practical Considerations.

17 A. Rose. The sensitivity performance of the human eye on an absolute scale. J. Opt. Soc. Am. 38, (1948) 196±208.

18 G. C. E Burger.The perceptibility of details in Roentgen examinations of the lung,. Acta Radiol. 31, (1949) 193±222.

19 G. A. Hay, O. F. Clark, N. J.Coleman, A. R. Cowen. A set of X-ray test objects for quality control in talevision ¯horoscopy. British Journal of Radiology 58, (1985) 335± 344.

20 C.J. Martin , P.F. Sharp, D.G. Sutton. Measurement of image quality in diagnostic radiology Applied Radiation and Isotopes 50 (1998) 21±38.

21 K. J Robson, C. J. Kotre, K. Faulkner,. The use of a contrast detail test object in the optimization of optical density in mammography. British Journal of Radiology 68, (1995) 277±282.

22 IPSM, Institute of Physical Sciences in Medicine. The commissioning and routine testing of mammographic X- ray systems. IPSM report 59, (1994) 2nd Edn. IPSM, York

23 R. Fahrig, J. Rowlands, M. Yaffe. X-ray imaging with amorphous selenium: optimal spectra for digital mammography, Med Phys. 23(4): (1996) 557-67.

24 V. Palmieri, G. Keppel, I. Kulyk, D. Tonini: "Engineering Of Magnetron Sputtering Sources For Thin Film Deposition"; Proceedings of XVII AIV congress, Venezia Lido 28/06/04 – 02/07/04.

25 W.S Rasband, ImageJ, U. S. National Institutes of Health, Bethesda, Maryland, USA, http://rsb.info.nih.gov/ij/, 1997-2006.

26 K. Cranley, B. J. Gilmore, G.W.A Fogarty and L Desponds. Catalogue of Diagnostic X-ray Spectra and other data. Produced for the Diagnostic Radiology and Magnetic Resonance Special Interest Group of the Institute of Physics and Engineering in Medicine.

27 Y. G. Shen, Y. W. Mai, Q. C. Zhang, D. R. McKenzie, W. D. McFall, W. E. McBride, Journal of applied physics; 87,1; January 2000.